Arabian Journal of Geosciences (2020) 13: 502
https://doi.org/10.1007/s12517-020-05394-8

S. I. GSF 2018

Updating a probabilistic seismic hazard model for Sultanate of Oman

Ahmed Deif[1] · Issa El-Hussain[1] · Yousuf Alshijbi[1] · Adel Mohamed El-Shahat Mohamed[1]

Received: 18 July 2019 / Accepted: 30 April 2020 / Published online: 18 June 2020

Abstract
Earthquake Monitoring Center (EMC) at Sultan Qaboos University (SQU) initiated evaluating the seismic hazard in the Sultanate of Oman in 2009. EMC has produced the first probabilistic and deterministic seismic hazard maps for Oman in 2012 and 2013, respectively. In the current study, the probabilistic seismic hazard assessment (PSHA) is revisited to provide an updated assessment of the seismic actions on the Sultanate. The present study has several advantages over its predecessor: using an updated homogeneous earthquake catalogue, recently developed seismic source model; inclusion of epistemic uncertainties for the source models, recurrence parameters, maximum magnitude, and more recent and applicable ground-motion prediction equations (GMPEs). Epistemic uncertainties were treated using a combination of the best available databases within a properly weighted logic tree framework. Seismic hazard maps in terms of horizontal peak ground acceleration (PGA) and 5% damped spectral accelerations (SA) at the bedrock conditions (VS = 760 m/s) for 475- and 2475-year return periods were generated using the classical Cornell-McGuire approach. Additionally, uniform hazard spectra (UHS) for the important population centers are provided. The results show higher values at the northern parts of the country compared to the hazard values obtained in the previous study.

Keywords Probabilistic · Seismic hazard · Updated · Oman

Introduction

The Sultanate of Oman occupies the northeastern part of the Arabian Peninsula in a convergence area amidst the Arabian and the Eurasian Plates. Main tectonic elements of this area is controlled by the collision of the two plates along the Bitlis-Zagros Fold-Thrust Belt northward movement of the Arabian Plate below the Eurasian Plate at the Makran Subduction Zone, the Owen Fracture Zone, and the Gulf of Aden (Fig. 1). Although Oman Mountains demonstrate some geologic and seismological indications for recent tectonic deformation (Ambraseys and Melville 1982; Kusky et al. 2005; Deif et al. 2017), most earthquake actions on the Sultanate are remote, occurring along the above four active tectonic trends as illustrated by the high rate of the earthquake activity (Fig. 2). These seismotectonic settings clearly imply that effective earthquake actions from regional and local seismic sources are possible and can generate significant damage to structures in Oman as indicated by the earthquake history of the Sultanate, emphasizing the necessity for earthquake catastrophe resilience of Omani structures (Ambraseys and Melville 1982; Ambraseys et al. 1994; Deif et al. 2013). Owing to the increasing development, rapid urbanization and huge investments in local and regional strategic projects, a heightened interest toward earthquake risk reduction has become an essential socioeconomic interest in Oman.

Accurate seismic hazard assessment is broadly considered as the most effective way toward earthquake risk mitigation (Giardini et al. 1999), as it is a necessity to build reliable earthquake resistance design codes for any country. PSHA is conducted at any site by taking into account all ground

This article is part of the Topical Collection on *Seismic and Earthquake Engineering Studies in the Arabian Plate and the Surrounding Region*

✉ Ahmed Deif
adeif@hotmail.com

Issa El-Hussain
elhussain@squ.edu.om

Yousuf Alshijbi
alshijbi@squ.edu.om

Adel Mohamed El-Shahat Mohamed
geotec_04@yahoo.com

[1] Earthquake Monitoring Center, Sultan Qaboos University, Muscat, Sultanate of Oman

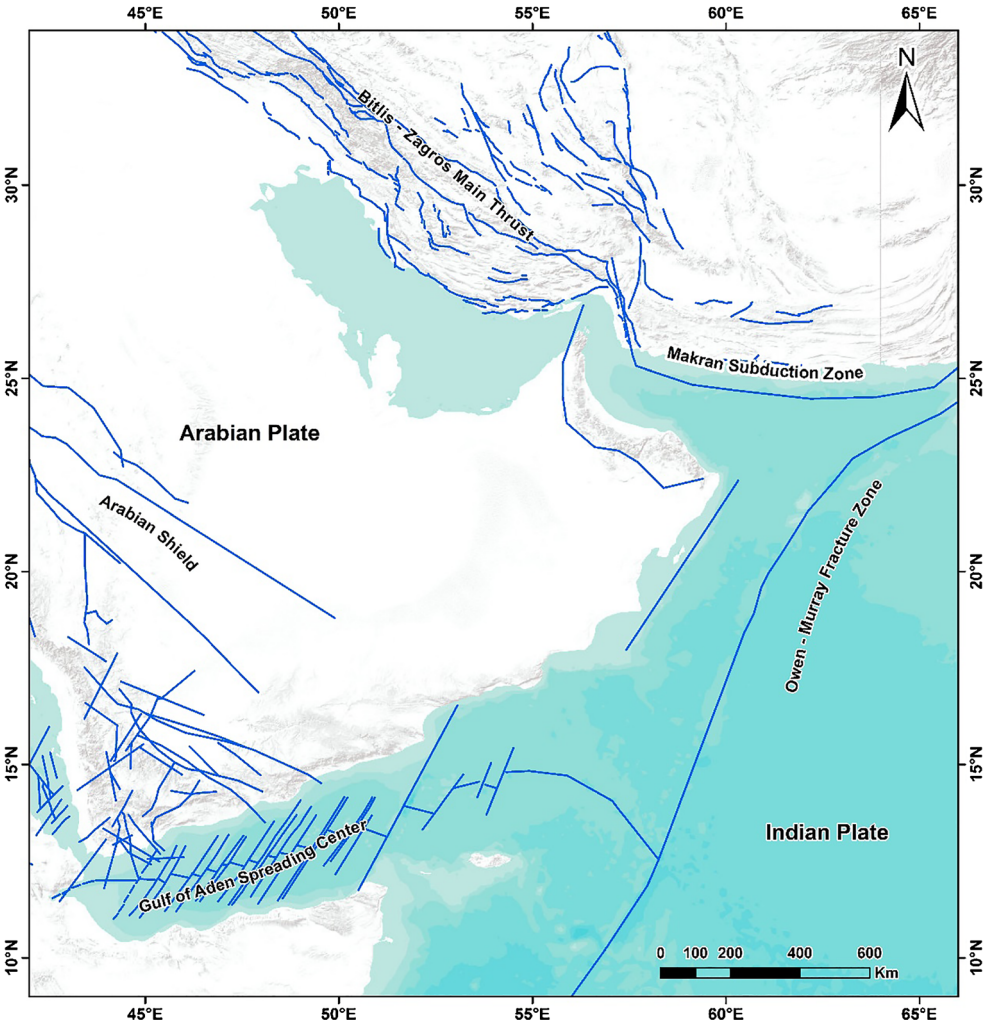

Fig. 1 Major tectonic elements in and around Sultanate of Oman

motions generated by a wide spectrum of earthquake magnitudes and distances from the effective seismic sources to develop a model of the earthquake-generating process. Uncertainties should be considered in each step of analysis. PSHA has the privilege of fully analyzing the aleatory variabilities and epistemic uncertainties. An additional advantage of PSHA is that it can be extended to evaluate seismic risk, defining the potential of losses caused by earthquakes, whether human, economic, social, or indirect ones.

Seismic hazard estimates were not available for Oman until 2012–2013, when the first probabilistic and deterministic hazard maps were published (El-Hussain et al. 2012; Deif et al. 2013), in response to the intention of Oman government to fill this gap and to improve the ability of the country to recognize the various levels of seismic hazard throughout the Sultanate. These two studies used seismic data extended from 734 AD up to 2010 AD. Since then, some large earthquakes occurred within the affecting seismic zones and compiled by Deif et al. (2017). Therefore, earthquake activity at all seismic sources that might affect the Sultanate of Oman needs to be updated based on new data acquired recently. Moreover, Earthquake Model of the Middle East (EMME) Project suggested different ground motion prediction equations (GMPEs) to be used in the Middle East. In this paper, new probabilistic seismic hazard analysis is presented, including the analysis of newly compiled catalogue (Deif et al. 2017), revised seismic source model, and selection of alternative ground motion prediction equations based on the results of several recent studies that published within the framework of the EMME project.

In the present paper, PSHA is undertaken using EZ-FRISK8.0b software developed by FUGRO-USA. Both aleatory and epistemic uncertainties were analyzed in the current hazard calculations. The aleatory variability due to actual random effect is included in the hazard evaluation by directly integrating the corresponding probability density functions within particular standard deviations. Epistemic uncertainties were considered using the "logic tree" algorithm (Coppersmith and Youngs 1986). In this algorithm, when any uncertainty appears, various alternatives are represented by separate branches on the logic tree and as fact-based as

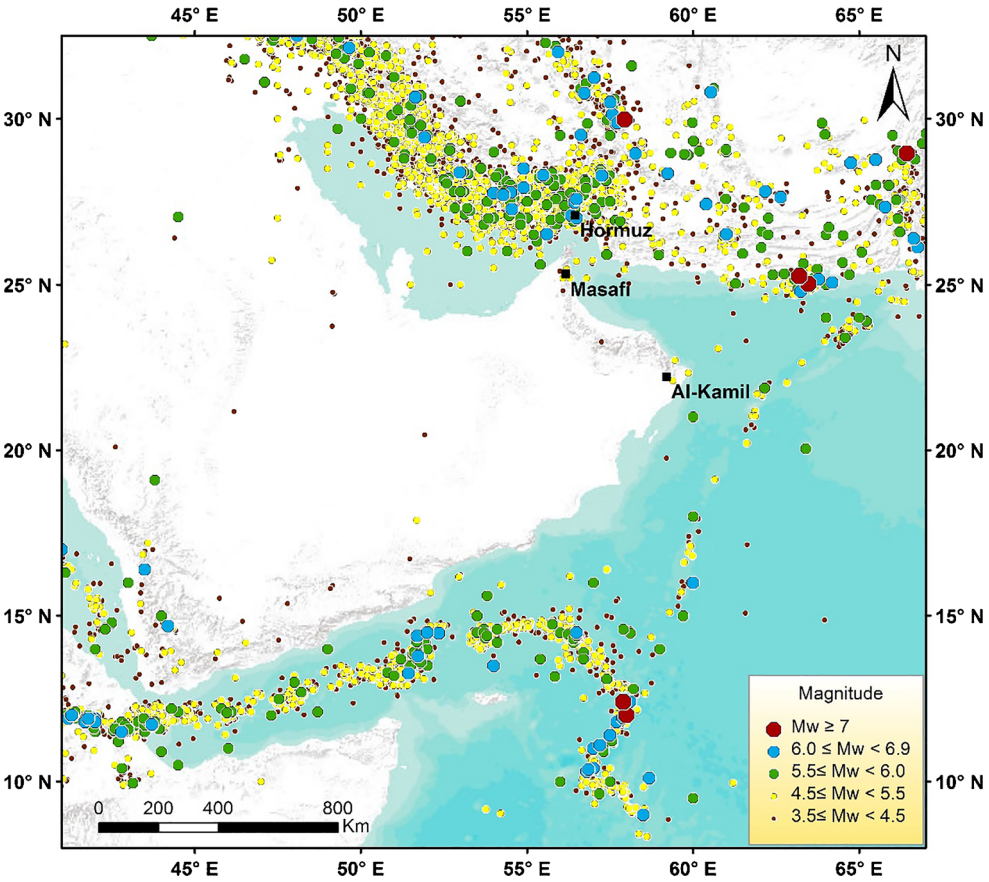

Fig. 2 Spatial distribution of instrumentally recorded earthquake activity (1900–2017) in and around Oman

possible weights are given to every single branch revealing the relative robustness of each raised alternative.

This study is focusing on providing updated seismic hazard values at bedrock conditions in the Sultanate of Oman for the purpose of reliable seismic resistant designs. Seismic hazard maps in terms of horizontal peak ground acceleration (PGA) and 5% damped spectral acceleration (SA) for 475- and 2475-year return periods are presented at the nodes of 0.1° regular grid. At this stage, results could be complemented by comprehensive site characterization studies at important facilities (e.g., Mohamed et al. 2008; El-Hussain et al. 2013). This gives additional flexibility to decision makers and engineers to choose the suitable level of conservatism according to the significance of the project of interest.

Seismotectonic setting of Oman and surrounding

Oman is bordered by four major tectonic structures comprising the Zagros Fold-Thrust Belt and Makran subduction zones to the north and east, the Gulf of Aden to the south, and Murray Ridge and Owen Fracture Zone to the east and southeast, respectively (Fig. 1). Additionally, Oman Mountains witnessed the occurrence of some small to moderate earthquakes and show some evidences for young topographic features, indicating recent tectonic activities (Kusky et al. 2005).

The seismic activity inside Oman is very low, and the majority of earthquakes take place at the boundaries of the Arabian Plate. Only three pre-instrumental earthquakes were reported to be occurred in Oman. In 879 AD, an earthquake was felt in Sohar without more details. It is unknown whether this earthquake is originated inside Oman or distant away in one of the surrounding seismic sources. The second earthquake occurred in 1483 and is ambiguously located in Western Makran with *Ms* 7.7 (Ambraseys and Melville 1982). The earthquake allegedly destroyed the city of Qalhat. Musson (2009) suggested that Qalhat was damaged in 1497 by another local earthquake with magnitude 6.0 and the earthquake of 1483 took place in Hormuz (south of Iran) as indicated by the numerous foreshocks that felt there. The third reported historical earthquake occurred in 1883 with *Ms* 5.1 and strongly felt in Muscat and Nizwa, damaging several villages in the vicinity of Nizwa. It is allegedly reported that the land was deformed at some sites. This clarification on historical earthquakes in Oman demonstrates that the location, size, and effects on people and their properties of the three reported earthquakes are uncertain.

Only two moderate size instrumentally recorded earthquakes occurred in the Oman Mountains. In 1971, an earthquake of magnitude 5.2 is located 12 km SSE of Al-Kamil City (Middle of Oman). This earthquake was surprisingly not felt, suggesting that the epicentral location is incorrect or the macroseismic data was missing. The hypocenter of this earthquake is determined utilizing few remote stations (distance ranges from 10° to 87°), thus reducing the credibility of its location. In March 2002, the second earthquake occurred in Masafi (most north part of the Oman Mountains) with magnitude 5.1 and felt broadly in northern Oman and the United Arab Emirates. This moderate size event could be considered as the only certain event in the Oman Mountains of that size.

Makran subduction zone is a large accretionary prism stretching E–W for about 900 km from southern Iran in the west to near Karachi in Pakistan in the east. It was created due to the northward movement of the oceanic part of the Arabian Plate beneath the Eurasian Plate since the early Tertiary, forming the boundary between the two plates (Kopp et al. 2000). Existing well-controlled focal mechanisms verify the thrust faulting of Makran zone (Deif et al. 2017). Most GPS measurements reveal constrained slip rate in the range of 19.5 ± 2 to 27 ± 2 mm/year (e.g., Vernant et al. 2004; ArRajehi et al. 2010). Makran zone has a very low angle subduction, with a trench dissimilar to any other trench in the world. Broad erosion of the Himalayan Mountains and the various waterways that stream into Oman Sea have covered the trench with deposits up to 7 km thick.

The seismicity of Makran zone is low compared with other Benioff zones. Historical and instrumental seismic records indicate that the eastern and western sections of Makran region have different patterns of earthquake activity. Almost every single large quake is reported to have taken place in the eastern section, suggesting segmentation. This segmentation is supported by many other geologic and tectonic features, indicating that a single seismic event breaking whole Makran zone is out of reach (Musson 2009). These features includes the offsets in the volcanic arcs, the large-scale two block structures of the overriding plate, and the presence of the NW trending sinistral fault of Sonne, which imputes the easternmost part of the Arabian Plate to separate it from the remaining Arabian Plate. The most recent large earthquake of Makran occurred at the Iran and Pakistan border with magnitude 7.6 in 2013. However, the most prominent seismic event was 1945 earthquake with moment magnitude 8.1. It was a tsunamigenic event that killed about 300 people (Ambraseys and Melville 1982). The tsunami was recorded along the coasts of Iran, Pakistan, as well as in Muscat.

The Zagros Fold-Thrust Belt is a 1500-km collision zone between the Arabian and Eurasian plates, extending from the East Anatolian Fault to the Benioff zone of Makran. The closest distance of Zagros to Northern Oman is less than 80km, indication that large earthquakes in this seismic zone may cause serious damage for structures in northern Oman. The collision is characterized by fairly high seismic activity, which may generate seismic hazard to neighboring countries. This active zone consists of a broad series of blind thrust faults covered by thick folded Phanerozoic deposits. The inner deformation between the northern and central Zagros zones is accommodated by a series of N-S strike-slip faults oblique to the main trend of the belt (Berberian 1995) (Fig. 3). Reilinger et al. (2006) used intensive GPS measurements to define a compression movement along the whole zone with a displacement of 23 ± 1 mm/year at the southern segment, and 19 ± 1 mm/year to the north.

Most earthquakes of Zagros Fold-Thrust Belt are of shallow depths (less than 20 km) and caused by high-angle reverse blind faults (30°–60°) without co-seismic surface traces (e.g., Hessami et al. 2006; Deif and El-Hussain 2012). This shallow focal depth implies that moderate to large earthquakes occur in the uppermost part of the Arabian basement (e.g., Baker et al. 1993; Hessami et al. 2001). There is no historical evidence for great earthquakes in the Zagros Fold-Thrust Belt, where earthquakes rarely exceed a magnitude of 7.1.

The Gulf of Aden is an oblique rift tectonic structure as its ENE-WSW trend is slanting to the NE-SW relative movement between Somalia and Arabian Plates. It runs along this divergent boundary from the Owen Fracture Zone toward the east to Djibouti toward the west (Fig. 1). Rifting of the Gulf of Aden is started about 35 Ma ago because of the northeast separation of the Arabian plate from the African plate with a slip rate of 20 mm/year (ArRajehi et al. 2010). This expansion in the end allowed the ocean bottom spreading since 18 Ma ago in the eastern section of the Gulf and propagated westward. Most of the gulf's floor is oceanic crust (Coleman 1993). Sheba Ridge spreading center is the main tectonic element in the gulf and is distinguished by many distinct NE striking transform faults. Among these faults, Alula-Fartaq is the most prominent as it dislocated Sheba Ridge for more than 150 km (Bosworth et al. 2005).

The earthquake activity in the Gulf of Aden is focused on its central area, along which the ocean bottom rifting takes place (Fig. 2). Much fewer seismic events occur at the northeast part of the gulf, which instigated El-Hussain et al. (2012) to consider this part as a separate seismic zone. The greatest detected event at the Gulf of Aden occurred in 2006 with *Mw* 6.6. Available focal mechanisms propose predominant normal with strike–slip faulting process, affirming the seismic activity of the central axis and the perpendicular transform boundaries (Deif et al. 2017).

The Indian Plate moves slightly slower than the Arabian Plate toward the north, colliding the southern margin of the Eurasian Plate. This dissimilarity in the rate of plate motions is accommodated by the Owen and the Murray seismic zones. These two seismic zones are about 1100-km-long dextral transform faults and both together constitute the Owen Fracture Zone. It stretches along the eastern border of the Arabian Plate with a slip rate of 3 mm/year (DeMets 2008; Akkar and Bommer 2010). ArRajehi et al. (2010) divided the

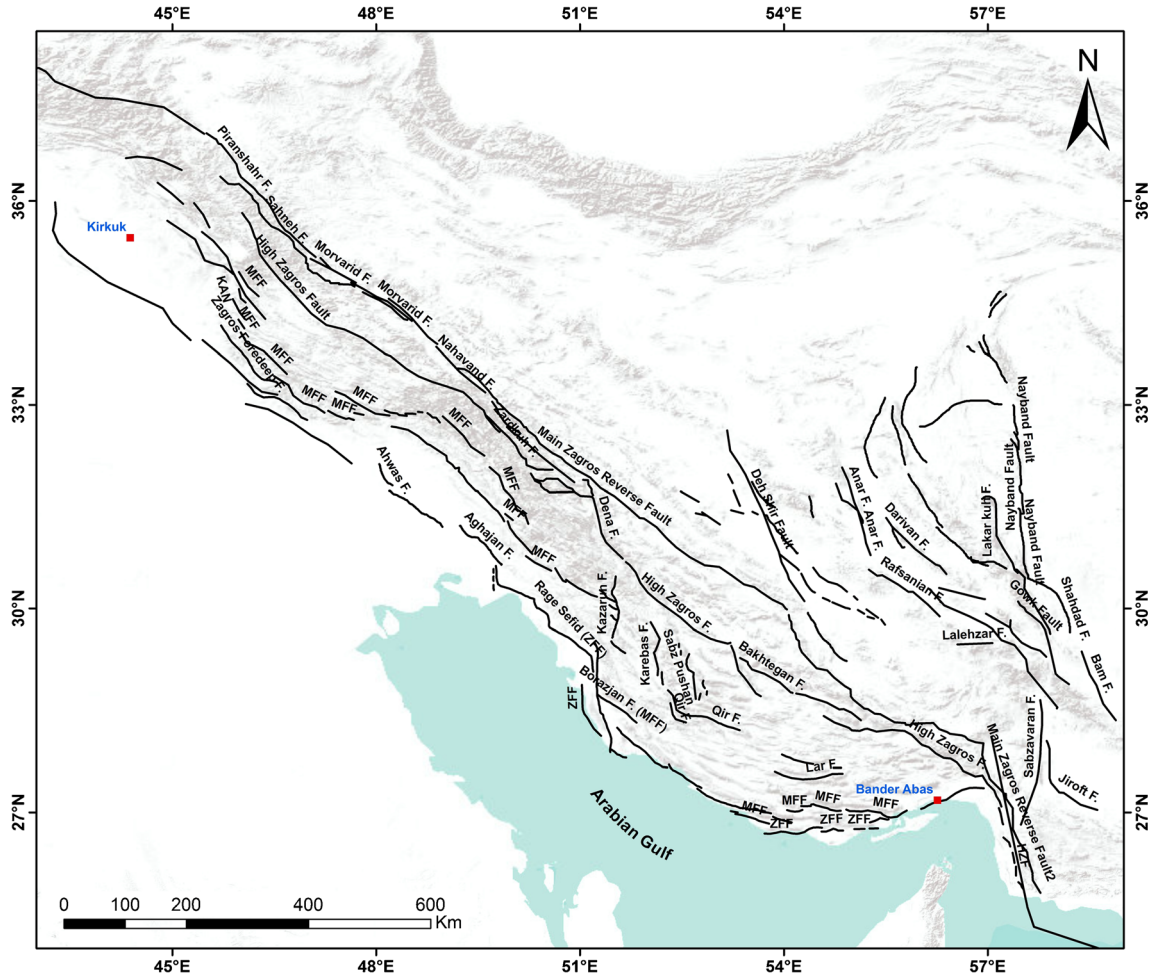

Fig. 3 Active faults of Zagros Fold-Thrust Belt (after Deif and El-Hussain 2012)

total current tectonic motion along Owen Fracture Zone to right lateral motion of about 3.2–2.5 ± 0.5 mm/year, and about 1–2 mm/year extension. As a result of this extremely low rate of plate motion, the earthquake activity on these two structures is not anticipated to be high. The largest documented earthquake along Owen and Murray seismic zones are *Mw* 6.6 and 5.8, respectively (Deif et al. 2017). Seismic activity on Owen fracture zone is mostly characterized by shallow earthquakes, with depth of focus not more than 15 km. Accurate fault plane solutions along Owen Fracture Zone show prevailing dextral faulting, and oblique normal sense of motion with a dextral faulting along Murray Ridge, in accordance with the faulting process proposed by ArRajehi et al. (2010).

Methodology

The main goal of PSHA is to calculate the probability that a specific ground motion level will be exceeded during a certain period of time at a particular site of interest due to all possible upcoming earthquake scenarios. PSHA in the current study has been conducted following the classical Cornell-McGuire approach (Cornell 1968, 1971; McGuire 1978) pioneered by Cornell (1968), including proper treatment of both aleatory and epistemic uncertainties of the ground motion. The procedure comprises two main models: a seismic source model and a ground motion model. The seismic source model describes the location and magnitude of future events, involving the definition of all seismic zones that can produce strong ground-shaking at the site of interest, the earthquake recurrence rate, and maximum credible magnitude at each zone. The ground motion model calculates the earthquake ground motion at a specific site as a result of all possible earthquake scenarios identified within the seismic source model. The classical Cornell-McGuire approach combines these two models to deliver hazard curves, expressing the variation of ground motion intensity versus annual frequency of exceedance.

Seismic source models

The present paper utilizes Al-shijbi et al. (2019) as a base for identifying the seismic source model for the Sultanate of

Oman. Two seismic source models were extracted from the two models developed in their study on seismic hazard assessment for the Arabian Peninsula (Fig. 4). They delineated the seismic source zones as seismically homogenous area sources, in which each point within a specific seismic source has the same potential of being the source of a future earthquake. The two seismic source models were identified based upon an updated earthquake catalogue (Deif et al. 2017), major structure elements, active faults, and their possibility to create effectual earthquakes, available geophysical data, as well as

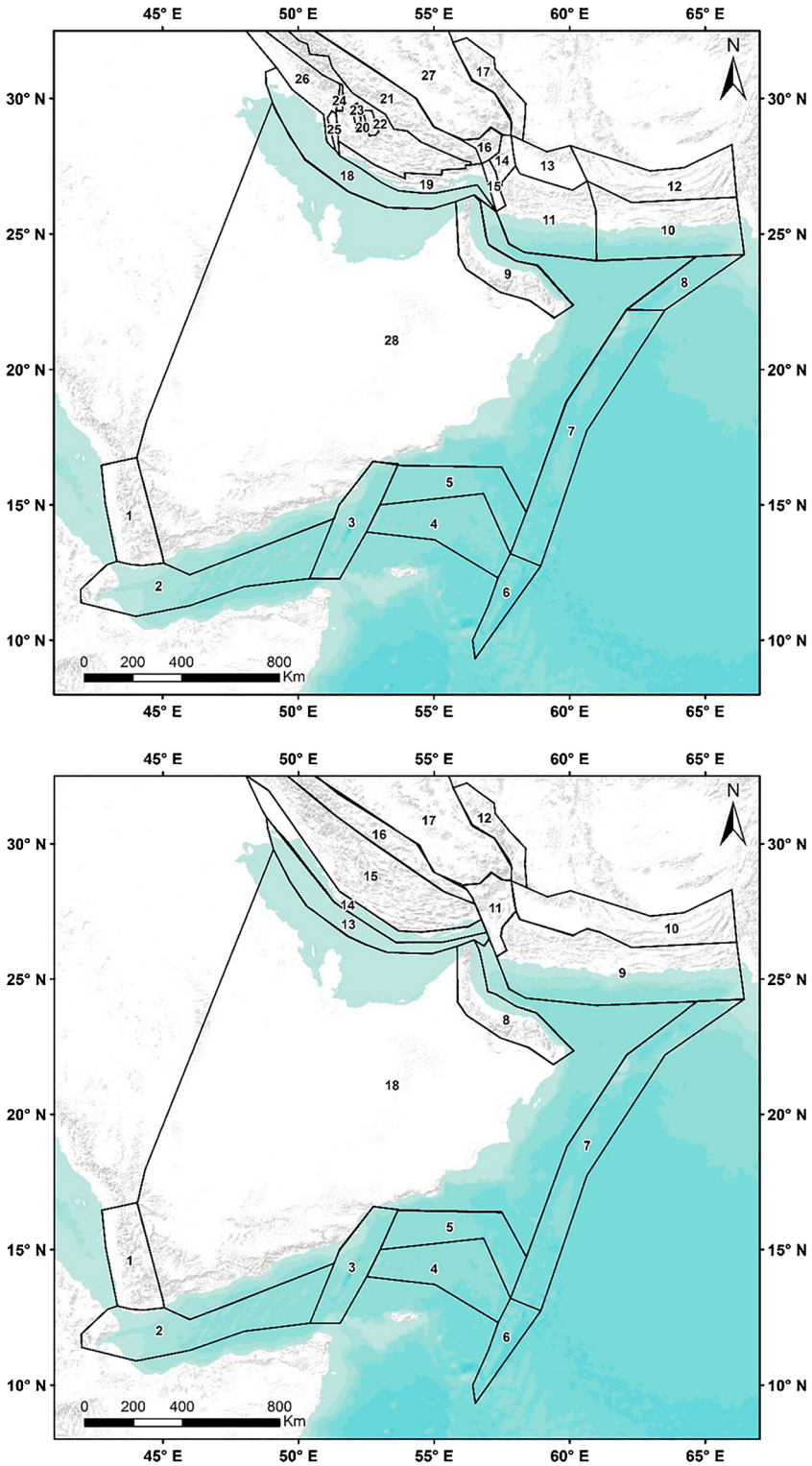

Fig. 4 Preferred (upper panel) and alternative (lower panel) source models used in the current study

previous studies. Seismic zones are mostly associated with the active major structures of Oman Mountains, Zagros, Makran, the transition zone between Zagros and Makran, Owen, and Gulf of Aden.

The first model has a higher resolution over the second model as it is more interrelated with the recognized distinct active faults with capability to produce significant seismic hazard in the Zagros Belt. The second model is generally utilizing greater zones, making an attempt to confine the main tectonic elements in and around Oman. The two alternative models represent Makran Subduction Zone in two different ways regarding its segmentation: The first model divides this seismic zone into two independent seismic sources (east and west sections), while the second model considers the entire Makran as one seismic source. Similarly, the first model splits Owen Facture Zone into Owen and Murray Ridge; however, the second model merges these two zones in one seismic source. Therefore, the authors lean toward preferring the first model and a higher weight, 0.8, is assigned to it, while a lower weight 0.2 is allocated to the second source model. The final seismic zones for each of the two selected source models are presented in Tables 1 and 2.

Deif et al. (2017) recognized the non-Poissonian earthquakes (foreshocks and aftershocks) and eliminated them from their earthquake catalogue utilizing Uhrhammer (1986) among other algorithms. They recommended using this declustered catalogue in seismic hazard study as it defines more events as independent ones and thus become more conservative. Additionally, they used Burkhard and Grunthal (2009) method to identify the time-based magnitude completeness. Their declustered catalogue and periods of completeness are used to calculate the recurrence parameters in the current study.

Recurrence relationships can define the probability of occurrence of a seismic event of a specific magnitude to hit anywhere within a particular source zone in a given period of time. They calculated the forthcoming seismic activity relying on the rates of earlier earthquake activity as estimated from their declustered catalogue. Gutenberg and Richter (1956) were initially introduced such relationship in seismology, defining an exponential recurrence distribution linking the accumulative number of earthquakes and the earthquake size. Unfortunately, their model is open at the lower and upper ends, instigating the unrealistic postulation that earthquake magnitude anywhere is boundless and unrelated to the limited extents of the causing faults. Therefore, the double-bounded exponential model of Cornell and Vanmarcke (1969) was followed herein to demonstrate the time-base distribution of earthquake occurrence at various magnitudes. In Cornell and Vanmarcke (1969) model, the annual number of earthquakes, $N(\mathrm{m} \geq M)$ equal to or greater than a particular earthquake magnitude M is mathematically expressed as:

$$N(\mathrm{m} \geq M) = \lambda \frac{\exp[-\beta(M-Mmin)]-\exp[-\beta(Mmax-Mmin)]}{1-\exp[-\beta(Mmax-Mmin)]} \quad (1)$$

where $\lambda = N(M_{\min})$, $M_{\min}$ is a random threshold magnitude reflecting the lowest earthquake size that might influence engineered structures; $M_{\max}$ is the upper-bound event that the earthquake source is able to produce, and $\beta = b \ln 10$, where b is the slope of Gutenberg and Richter (1956) relationship.

Owing to the different periods of completeness for various magnitude levels in the used earthquake catalogue, the coefficients of Cornell and Vanmarcke (1969) model cannot be estimated properly utilizing a direct regression. Therefore, these coefficients and their standard deviations were calculated for each seismic source applying the algorithm developed by Kijko and Sellevoll (1992), allowing various time periods of earthquake completeness for different magnitudes to be introduced. The recurrence parameters of Cornell and Vanmarcke (1969) model and their uncertainties for the two used source models (Fig. 4) are shown in Tables 1 and 2.

The maximum magnitude ($M_{\max}$) for a particular seismic zone is mainly calculated adopting the Kijko (2004) approach. This approach is thoroughly rely on statistics of the frequency of occurrence distribution of existing earthquake data, combining incomplete and relatively unrealistic data from historical periods with those obtained from complete and most reliable instrumental data. This approach is our favorite choice to determine $M_{\max}$; however, when insufficient earthquake data exist at a specific seismic zone, $M_{\max}$ is estimated by adding 0.5 magnitude units to the maximum reported magnitude in this particular seismic zone.

Concerning the parameters of the recurrence relationship [β, λ, and maximum magnitude ($M_{\max}$)] at each effective seismic source, the probabilistic seismic hazard assessment was conducted utilizing the mean values of the three parameters, as well as adding and subtracting one standard deviation, successively. The mean values are assigned a weight of 0.6, whereas weights of 0.2 are given the branches of recurrence parameters ± one standard deviation.

Additional uncertainty associated with the maximum earthquake in the Western Makran seismic zone is raised due to the earthquake in 1483. If this earthquake has actually taken place with M 7.7 in this segment according to Ambraseys and Melville (1982), the maximum magnitude is calculated to be 8.2. Alternatively, if this earthquake was a local one with M 6.0 close to Hormuz according to Musson (2009), the maximum expected magnitude would be 6.2 in Western Makran. The first alternative is allocated a weight of 0.3 as it relies on a relatively older research with ambiguous earthquake location (Ambraseys and Melville 1982), whereas the second hypothesis is given a weight of 0.7 as it is supported by the foreshocks activity preceded this event at Hormuz. A list of the

Table 1 Seismic sources and corresponding recurrence parameters for the preferred source model

Zone no.	Zone name	a	λ	$\sigma(\lambda)$	b	σb	β	$\sigma\beta$	M_{max}obs	M_{max}	σ M_{max}
Zone 1	Yemen	3.15	0.518	0.13	0.86	0.08	1.97	0.18	6.3	6.4	0.31
Zone 2	Western Aden	3.47	6.222	1.059	0.67	0.04	1.55	0.09	6.6	6.7	0.31
Zone 3	Alula-Fartaq	2.34	2.172	0.397	0.5	0.1	1.15	0	6.6	6.7	0.31
Zone 4	Eastern Aden	2.65	4.513	0.793	0.5	0.1	1.15	0	6.1	6.1	0.3
Zone 5	Northeastern Gulf of Aden	1.83	0.357	0.13	0.57	0.09	1.31	0.21	5.8	6.2	0.48
Zone 6	Southern Owen	2.61	2.127	0.358	0.57	0.05	1.31	0.11	7.1	7.2	0.33
Zone 7	Owen	2.05	0.594	0.16	0.57	0.08	1.31	0.24	6.5	6.8	0.24
Zone 8	Murry Ridge	1.75	0.559	0.193	0.5	0.1	1.15	0	5.9	6.1	0.25
Zone 9	Oman Mountains	2.71	0.243	0.08	0.83	0.09	1.94	0.21	6.0	6.2	0.21
Zone 10	Makran East	2.98	1.822	0.371	0.68	0.06	1.57	0.14	8.1	8.4	0.1
Zone 11	Makran West	2.71	0.680	0.167	0.72	0.08	1.65	0.19	5.9	6.2	0.23
Zone 12	Makran Intraplate	2.53	0.860	0.198	0.65	0.06	1.49	0.16	7.3	7.8	0.3
Zone 13	Jaz-Murian	2.35	0.423	0.131	0.68	0.09	1.56	0.2	6.1	6.8	0.82
Zone 14	Jiroft Fault	3.06	1.268	0.271	0.74	0.07	1.70	0.17	5.8	6.0	0.14
Zone 15	Zendan Fault	1.95	0.465	0.133	0.57	0.09	1.30	0.2	6.1	6.3	0.22
Zone 16	Ali Abad	2.97	2.157	0.411	0.66	0.06	1.52	0.14	6.6	6.8	0.18
Zone 18	Arabian Gulf	3.30	1.821	0.368	0.76	0.07	1.74	0.16	6.1	6.2	0.26
Zone 17	Gowk Fault	3.12	1.602	0.299	0.73	0.06	1.68	0.13	7.2	7.5	0.34
Zone 19	Zagros Foredeep	3.69	3.359	0.52	0.79	0.05	1.83	0.11	6.7	6.8	0.21
Zone 20	Zagros Simple Fold	4.11	8.820	1.16	0.79	0.03	1.82	0.07	6.8	6.9	0.21
Zone 21	High Zagros	3.53	3.094	0.468	0.76	0.04	1.75	0.1	7.4	7.6	0.24
Zone 22	Sabz-Pushan Fault	2.76	0.686	0.184	0.73	0.08	1.69	0.19	6.1	6.3	0.34
Zone 23	Karebas Fault	2.62	0.314	0.104	0.78	0.09	1.81	0.22	5.4	5.8	0.46
Zone 24	Kazerun Fault	2.97	1.621	0.417	0.69	0.08	1.60	0.19	5.9	6.0	0.21
Zone 25	Borazjan Fault	2.80	0.989	0.281	0.7	0.08	1.61	0.19	5.7	5.8	0.22
Zone 26	Dezful Embayment	3.97	5.340	0.817	0.81	0.04	1.86	0.1	6.7	6.8	0.12
Zone 27	Iranian Background	3.5	1.15	0.215	0.86	0.05	1.99	0.11	6.7	6.7	0.27
Zone 28	Arabian Background	4.26	2.000	0.342	0.99	0.06	2.29	0.15	6.5	6.6	0.31

The minimum magnitude (M_{min}) = 4.0 for all zones

maximum observed and calculated magnitudes in each seismic zone is tabulated in Tables 1 and 2.

Ground motion model

A ground motion model mostly involves some carefully chosen ground motion prediction equations, calculating the expected ground motion intensity at a specific site based upon the magnitude and distance between the site and a particular seismic zone. GMPEs may be the input component with the largest impact on the final results of seismic hazard assessment. Selection of appropriate GMPEs for an area of interest is one of the major sources of epistemic uncertainty in any seismic hazard study (Toro 2006), where insufficient ground motion data exist to obtain area-specific models. Moreover, scattering associated with each GMPE could be defined in terms of standard deviation, which is in itself a substantial element reflecting the irregularity in ground motion.

The shortage of ground motion acceleration time histories in Oman instigated borrowing GMPEs previously developed in other parts of the world, in tectonic settings analogous to those around the Sultanate. The GMPEs of Zhao et al. (2006), Chiou and Youngs (2008), and Akkar and Bommer (2010) are used to model ground motions of active shallow seismic zones, while equations of Youngs et al. (1997), Atkinson and Boore (2003), and Zhao et al. (2006) are applied to demonstrate the ground motion behavior of Makran subduction zone events. The GMPEs of Atkinson and Boore (2006) with 140 bar stress drop and Campbell (2003) are principally utilized for the Arabian stable craton. Since it is not entirely certain that the Arabian Peninsula can be described as a stable craton (Aldama et al. 2009), a combination of the three active shallow GMPEs together with GMPEs of Atkinson and Boore (2006) and Campbell (2003) are used to model the ground motion of the Arabian Peninsula Zone. All GMPEs above can estimate the horizontal ground motion in terms of PGA

Table 2 Seismic sources and corresponding recurrence parameters for the alternative source model

Zone no.	Zone name	a	λ	$\sigma(\lambda)$	b	σb	β	$\sigma\beta$	M_{max}obs	M_{max}	σM_{max}
Zone 1	Yemen	3.07	0.52	0.165	0.84	0.09	1.94	0.2	6.3	6.9	0.79
Zone 2	Western-Aden	3.47	6.22	1.059	0.67	0.04	1.55	0.09	6.6	6.7	0.31
Zone 3	Alula-Fartaq	2.34	2.17	0.397	0.5	0	1.15	0	6.6	6.7	0.31
Zone 4	Eastern Aden	2.65	4.51	0.793	0.5	0	1.15	0	6.1	6.1	0.3
Zone 5	Northeastern Gulf of Aden	1.83	0.36	0.13	0.57	0.09	1.31	0.21	5.8	6.2	0.48
Zone 6	Southern Owen	2.61	2.13	0.358	0.57	0.05	1.31	0.11	7.1	7.2	0.33
Zone 7	Owen	2.40	1.00	0.234	0.6	0.07	1.39	0.16	6.5	6.7	0.28
Zone 8	Oman-Mountains	2.71	0.24	0.08	0.83	0.09	1.94	0.21	6.0	6.2	0.21
Zone 9	Southern Makran	3.10	2.20	0.392	0.69	0.05	1.59	0.12	8.1	8.4	0.2
Zone 10	Northern Makran	2.80	1.20	0.237	0.68	0.06	1.57	0.14	7.8	8.1	0.2
Zone 11	Transition Zone	3.38	3.80	0.604	0.7	0.04	1.62	0.1	6.6	6.7	0.22
Zone 12	Gowk-Fault	3.12	1.60	0.299	0.73	0.06	1.68	0.13	7.2	7.5	0.34
Zone 13	Arabin Gulf	2.61	0.71	0.175	0.69	0.08	1.59	0.19	5.8	6.0	0.26
Zone 14	Zagros-Foredeep	4.20	3.00	0.467	0.93	0.04	2.14	0.1	7.3	7.6	0.35
Zone 15	Zagros Simple Fold	4.27	9.75	0.858	0.82	0.02	1.89	0.05	6.8	6.9	0.21
Zone 16	Zagros main thrust	4.12	2.75	0.381	0.92	0.04	2.11	0.09	7.4	7.7	0.4
Zone 17	Iranian Background	3.5	1.15	0.215	0.86	0.05	1.99	0.11	6.7	6.7	0.27
Zone 18	Arabian Background	4.26	2.00	0.342	0.99	0.06	2.29	0.15	6.5	6.6	0.31

and 5% damped spectral acceleration (SA). They are globally utilized for seismic hazard assessment and have been validated for use in the Middle East (Delavaud et al. 2012; Douglas et al. 2014).

Combining more than one GMPE in a logic tree in seismic hazard analysis necessitates some modifications due to the diverse descriptions existing for the input and output parameters of GMPEs. Thus, all alternative branches of the logic tree have to be converted to common metrics (Bommer et al. 2005; Al-shijbi et al. 2019). The compatibility of the above GMPEs regarding earthquake size, the distance between the source and site of interest, and definition of the used horizontal component were carefully considered to apply these GMPEs within a single logic tree.

For GMPEs applied for active shallow zones, the model of Akkar and Bommer (2010) is given the highest weight of 0.5. This is adopted as these relationships are rather more recent, utilized many recordings of strong-motion stations installed in the Middle East, and is selected among the GMPEs that are suitable for the area of interest (Delavaud et al. 2012). Models of Zhao et al. (2006) and Chiou and Youngs (2008) are allocated even weights, 0.25. For Makran subduction zone, the model of Zhao et al. (2006) is preferred over others with a weight of 0.5, while the residual weight 0.5 is evenly distributed between Youngs et al. (1997) and Atkinson and Boore (2003) models. Regarding the GMPEs applied for the allegedly stable Arabian craton, the relationships of Atkinson and Boore (2006) and Campbell (2003) are favored with weights of 0.3 and 0.25, respectively. The residual weight 0.45 is equally divided among the other three active shallow zones models.

In compatibility with the used earthquake catalog, moment magnitude scale expresses the earthquake size in all applied GMPEs. Therefore, there is no need for any conversion among different magnitude scales. Akkar and Bommer (2010) use RJB as a definition for the distance between the seismic source and the site of interest in contrast to the remaining GMPEs, which make use of Rrup. Fortunately, in EZ-FRISK 8.0b, the GMPEs can be entered as tables contain the level of the selected ground motion parameter at certain magnitude and distance pair. This permits various definitions of distance to be used synchronously without further distance amendments. Horizontal ground motion is identified in the current study as the geometric mean of the two horizontal components. GMPEs for which the horizontal ground motion is not recognized in the same metric are converted into this classification by means of the models developed by Beyer and Bommer (2006).

Results

Following the logic tree algorithm, seismic hazard is calculated separately for each branch. Weightings of all nodes along the targeted branch are multiplied together in order to obtain the ending-weight for the hazard results of each specific computation. The final hazard results in the present study are then evaluated utilizing a weighting average technique with the

intention to calculate a hazard curve for each node. This process is repeated for each ground-motion parameters of interest (PGA and SA at different spectral periods). The logic tree of the current study includes five components involving, seismotectonic source models, maximum magnitude of western Makran seismic zone, recurrence parameters with their standard deviations, the maximum magnitudes in each seismic zone with their standard deviations, and ground motion prediction equations.

Seismic hazard is calculated at rock site conditions referring to the site classification of the National Earthquake Hazards Reduction Program (V_{S30} = 760 m/s). V_{S30} is the mean velocity of shear-waves in the topmost 30 m of the site. Arbitrary M_{min} equals 4.0 is selected to be utilized for seismic hazard assessment, as earthquakes smaller than this threshold are believed incapable to influence engineered structures, and thus are not taken into account in the current hazard assessments. The principal hazard results of this study are represented in terms of hazard curves, uniform hazard spectra (UHS), deaggregated products for return periods of 475 and 2475 years at the most populated 12 cities in Oman, as well as seismic hazard maps for the entire country. Seismic hazard curves are the outcome of PSHA at a single site and hazard maps for a particular region can be accomplished through simultaneous hazard assessment at various sites in the region and creating iso-maps for specified ground-motion parameter at a given return periods. Only selected portions of the results are revealed in the following sections as the whole hazard results for the considered ranges of frequencies and return periods, comprising UHS are available on the following website: https://www.squ.edu.om/emc/Oman_hazardmaps.

Seismic hazard curves

A hazard curve shows the annual frequency that a given threshold ground motion level is exceeded at a specific site owing to the forthcoming earthquakes. Seismic hazard results at the bedrock conditions are created in terms of Hazard curves of PGA and 5% damped SA for 12 main cities in Oman namely from south to north Salalah, Duqum, Haima, Sur, Nizwa, Ibri, Rustaq, Muscat, Buraimi, Sohar, Diba, and Khasab (Fig. 5). Seismic hazard curves in terms of peak ground acceleration for the 12 selected cities that cover the entire country and represent various geologic and seismic environments are plotted in Fig. 6a, b for the northern and southern cities, respectively. PGA seismic hazard curves for the 12 cities indicate low seismic hazard in most of the territory with relatively higher levels for cities near Zagros and Makran seismic source zones.

The highest hazard level is observed at Khasab City at the most northern part of the country due to the proximity of the Zagros and Makran seismic zones, which are the most active zones in the region. The hazard levels at Haima and Duqm cities are very similar, revealing the lowest hazard among the selected 12 cities, as the two cities are located in the middle part of Oman away from the more active seismic zones and thus more being affected by seismic sources with low seismic activity (Arabian background zone). Hazard values in Salalah, Sur, Nizwa, and Muscat cities show little variability and the hazard curves converge at long return period where the low active local seismicity of Oman Mountains' zone controls the hazard. For the east northern cities (Rustaq, Sohar, Diba, and Khasab), the seismic hazard increases northward and the hazard curves converge at long return periods as Oman Mountains seismic source with relatively lower activity dominates the results. The two northwestern cities (Ibri and Buraimi) have almost the same PGA level along the entire range of return period. Spectral accelerations (SA) seismic hazard curves at 0.2s spectral period show the same behavior as PGA hazard curves albeit with higher values (Fig. 6c, d). The annual frequency of occurrence and return periods of fixed intensities of 50 and 100 cm/s^2 at cities of Salalah, Muscat, and Khasab prove the higher seismic activity toward north (Table 3).

Deaggregation of hazard curves

Seismic hazard curve of PSHA provides, jointly together, the influences of all possible future earthquake scenarios (magnitudes and distances) on the annual frequency of exceedance of a specific hazard level. In this way, the exceedance rates given by the seismic hazard curve are not correlated with any distinct earthquake scenario (Kramer 1996). In many design conditions, particularly for critical structures, it is more convenient to have the expected seismic action as the ground-motion time history of a specific scenario. Thus, the deaggregation process becomes essential as it defines how various earthquake scenarios impact the total seismic hazard at the site of interest for a given return period, including the earthquake scenario that controls the seismic hazard most. Consequently, a number of earthquake time histories can be obtained to develop the fragility curves.

The deaggregation process is performed computationally by reordering the parameters of the hazard equation with the intension to get the rate of exceedance of specific ground-motion intensity for a specific earthquake scenario. This can be written mathematically in the following form:

$$\gamma\left(Z > z|m_j, r_k\right) = \sum_{i=1}^{Nsource} v_i P\left(M = m_j\right) P(R = r_k) \int_{\varepsilon=-\infty}^{\infty} f_{\varepsilon}(\varepsilon) P\left(Z > z|m_j, r_k, \varepsilon\right) d\varepsilon \quad (2)$$

where νi is the rate of occurrence of earthquakes with magnitude greater than Mmin for source i, $P(M = m_j)$ and $P(R = r_k)$ are the probabilities that an earthquake with magnitude M at a distance R from the site of interest takes place in the seismic

source *i*, respectively, and ε is the number of standard deviations in the ground motion prediction equation needed to get the targeted ground-motion at a specific magnitude and distance.

Seismic hazard curves of PGA and 5% damped SA at 0.2, 1.0, and 2.0 s spectral periods were deaggregated at the selected 12 cities for hazard levels of 475- and 2475-year return periods which correspond to 10 and 2% probability of exceedance in 50 years, respectively. Deaggregation calculations are conducted on the mean values over all branches utilized for each site. Equal magnitude and distance spacing are used to depict the deaggregation findings. Figure 7 shows, as examples, deaggregation results for 475-year return period at Khasab, Sohar, Muscat, Duqum, and Salalah. All deaggregation results for the two selected hazard levels are shown in Tables 4 and 5 Generally, the obtained deaggregation results are different for different spectral periods and for different hazard levels as indicated in Tables 4 and 5.

For Salalah City and for 475-year return period, earthquakes with magnitude ranges from 6.25 to 6.75 at a distance of about 142 km (Alula-Fartaq seismic zone) influence most to the total hazard for all studied SA (Fig. 7 and Table 4). For 2475-year return period, the seismic hazard is controlled by near small to moderate-size earthquakes from the Arabian background source (within which Salalah City lies) for short spectral periods and by Alula-Fartaq seismic source with larger earthquakes for longer ones. This implies that the Arabian background seismic source needs a longer time to generate earthquakes capable to produce considerable effects at short spectral periods. For cities of Duqum, Haima, and Buraimi, which lies within the Arabian background seismic zone away from all other seismic sources, the resulted low seismic hazard is dominated by the nearby earthquakes for short SA periods

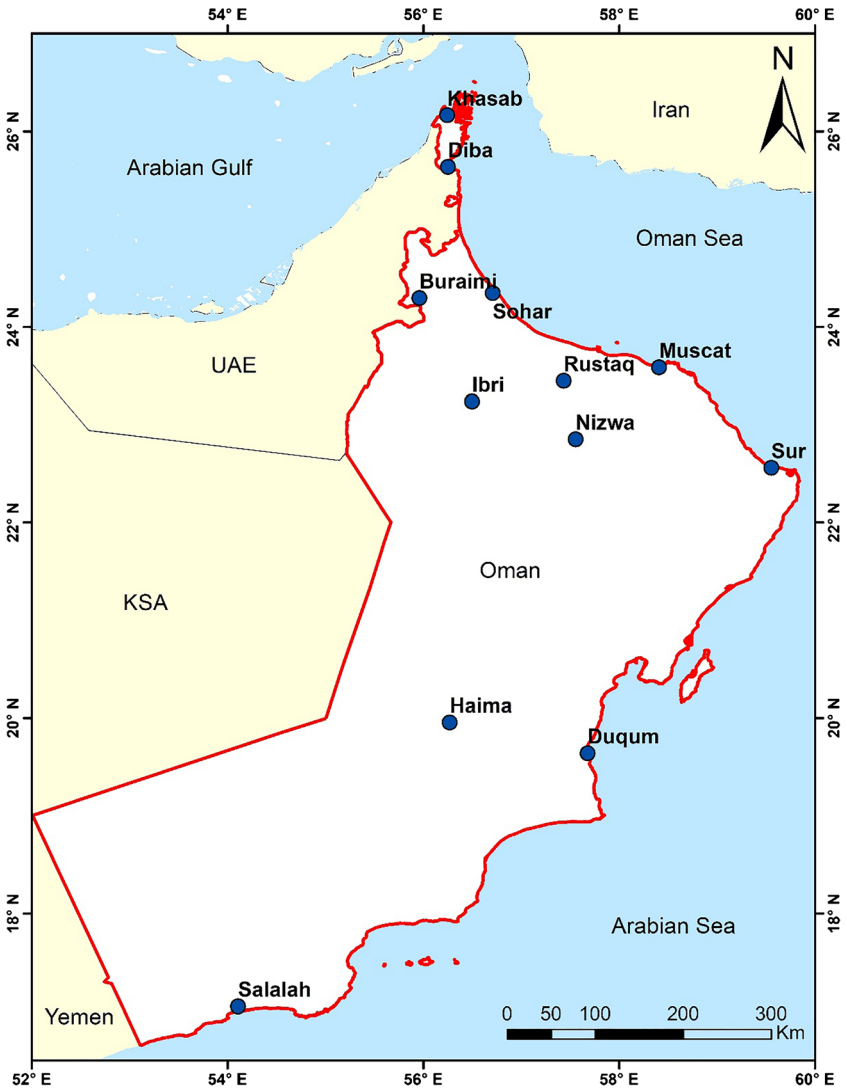

Fig. 5 12 selected cities for detailed PSHA

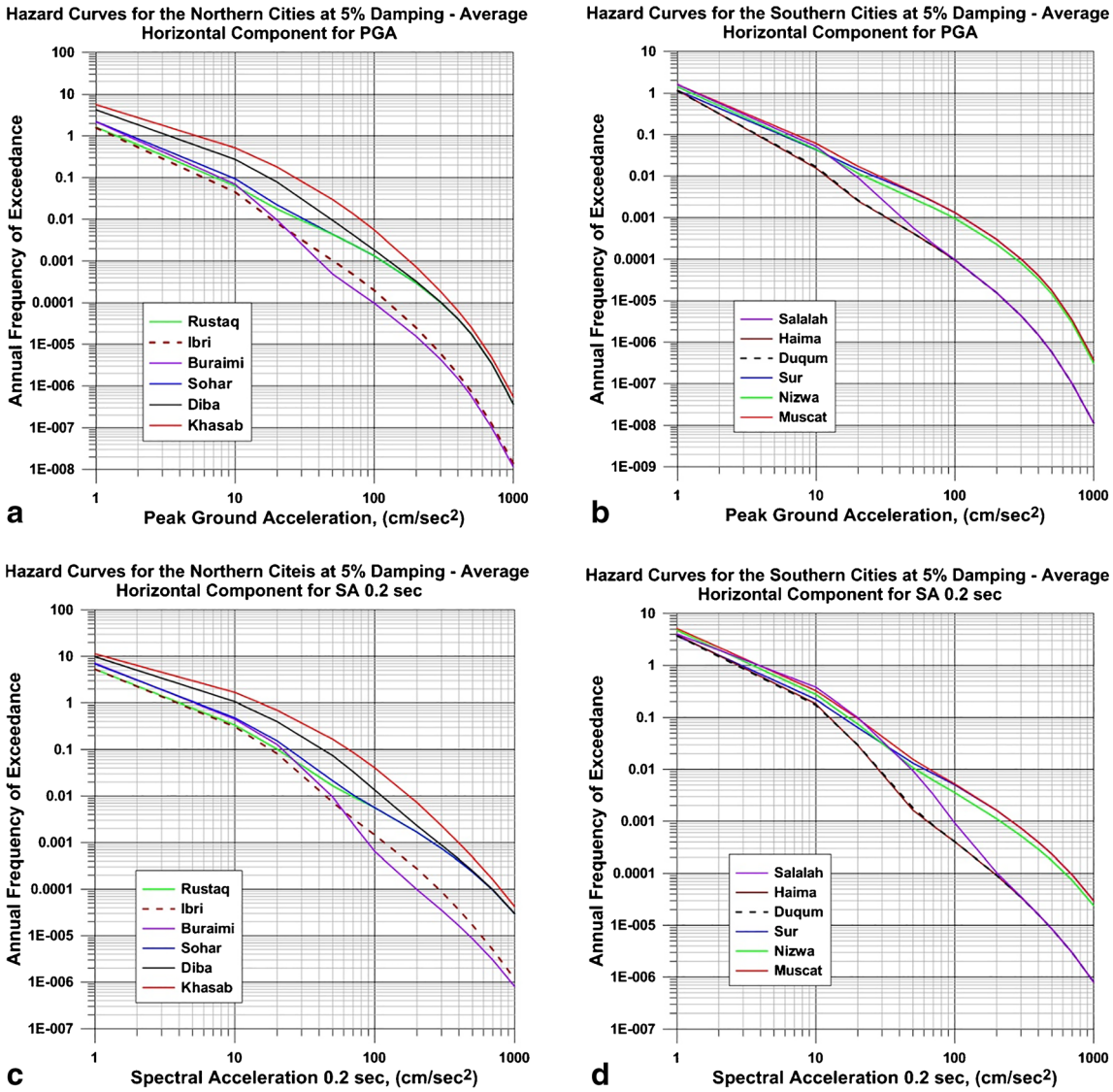

Fig. 6 Updates seismic hazard curves at the 12 selected cities for PGA (**a**, **b**) and 5% damped SA for 0.2 spectral period (**c**, **d**)

and by remote larger events for longer spectral periods. This points out to the low seismic activity rates of the Arabian background source and significant hazards from this source is not possible. With exception of SA at 2.0 s, nearby seismic sources dominate the seismic hazard at Nizwa City for 475- and 2475-year return periods.

Table 3 Annual frequency and corresponding return periods at Salalah, Muscat, and Khasab cities

City		Annual frequency of exceedance			Return period		
		PGA	0.2 s	1.0 s	PGA	0.2 s	1.0 s
Khasab	100 cm/s^2	0.0055070	0.0404530	0.0009339	181.584762	24.7197399	1070.69361
	50 cm/s^2	0.0298733	0.1674550	0.0086280	33.4747081	5.97175360	115.890566
Muscat	100 cm/s^2	0.0013201	0.0052530	0.0001449	757.483941	190.348200	6898.54992
	50 cm/s^2	0.0042092	0.0155940	0.0007270	237.572010	64.1268171	1375.33042
Salalah	100 cm/s^2	0.00009809	0.0009221	0.00001159	10193.8046	1084.44697	86230.6843
	50 cm/s^2	0.0005643	0.0094000	0.0001845	1771.81816	106.3738125	5417.61700

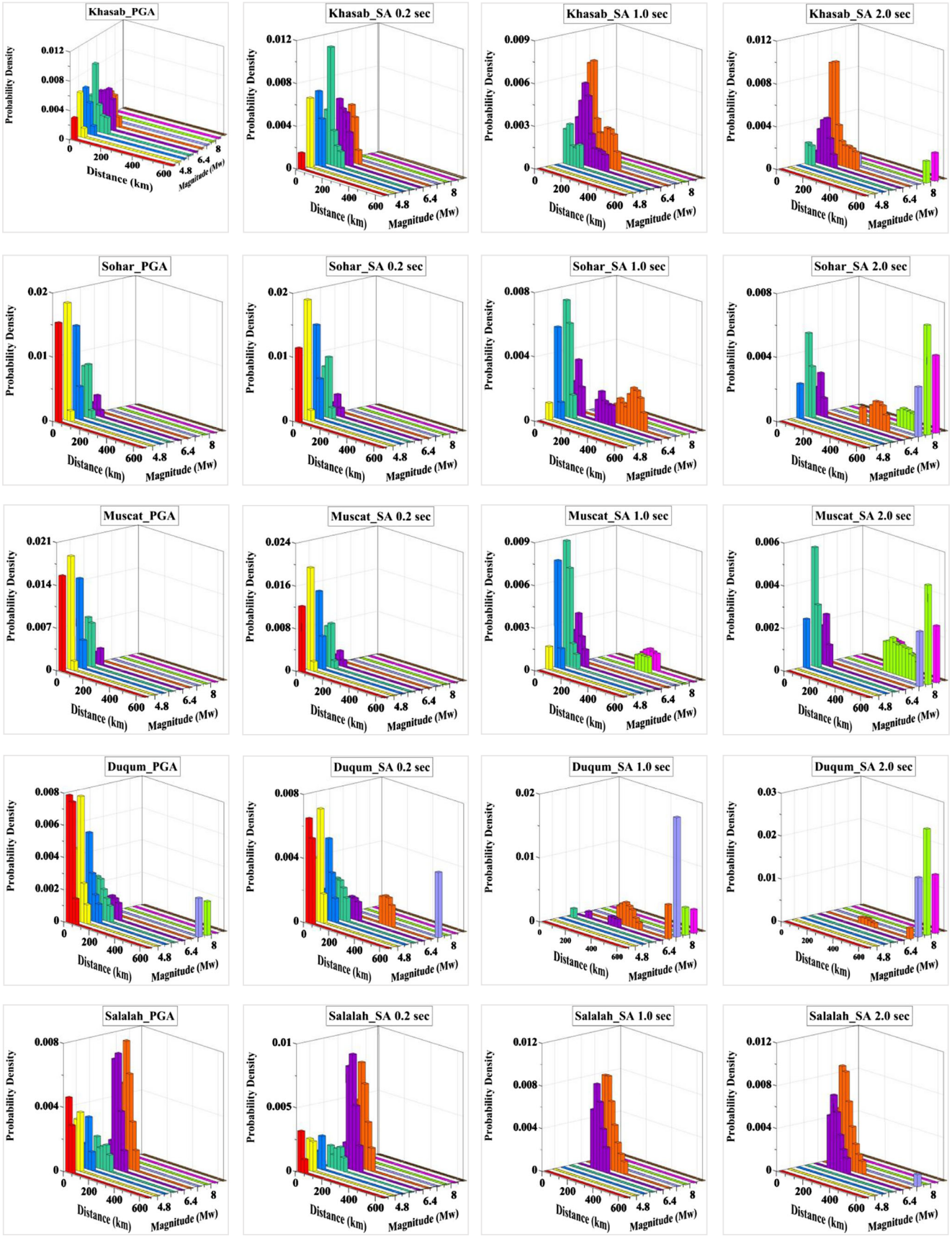

Fig. 7 Outcomes of deaggregation process at 5 cities (Salalah, Duqum, Muscat, Sohar, and Khasab), depicting the relative contribution of influencing seismic sources to the total hazard in terms of PGA and 5% damped spectral accelerations at 0.2, 1.0, and 2.0-s spectral periods.

Table 4 Deaggregation results in terms of mean and model magnitude and distance of the most contributing seismic source for the 12 selected cities for PGA and SA at 0.2, 1.0, and 2.0 s for 475-year return period

City	PGA				SA (T = 0.2 s)				SA (T = 1.0 s)				SA (T = 2.0 s)			
	Magnitude		Distance		Magnitude		Distance		Magnitude		Distance		Magnitude		Distance	
	Mode	Mean	Mode	Mean	Mode	Mean	Mode	Mean	Mode	Mean	Mode	Mean	Mode	Mean	Mode	Mean
Khasab	5.75	5.81	42.5	61.72	5.75	5.89	42.5	82.66	6.75	6.45	92.5	138.60	6.75	6.75	92.5	197.40
Diba	4.75	5.46	17.5	56.73	4.75	5.49	17.5	55.00	6.25	6.44	142.5	187.84	6.75	6.86	142.5	295.16
Sohar	4.75	5.12	17.5	28.31	4.75	5.25	17.5	55.19	5.75	6.44	17.5	270.40	7.75	6.97	642.5	403.80
Buraimi	4.25	5.91	17.5	189.78	6.75	6.16	292.5	223.65	6.75	6.69	292.5	373.79	7.75	7.14	642.5	534.61
Ibri	5.25	5.40	42.5	72.92	5.25	5.43	42.5	70.46	7.25	6.67	642.5	390.37	7.75	7.22	642.5	551.57
Rustaq	4.75	5.12	17.5	27.56	4.75	5.18	17.5	29.11	5.75	6.34	42.5	224.99	7.75	7.04	642.5	411.27
Muscat	4.75	5.12	17.5	30.23	4.75	5.18	17.5	34.06	5.75	6.70	17.5	276.10	5.75	7.19	17.5	373.80
Nizwa	4.25	5.05	17.5	29.71	4.75	5.10	17.5	31.79	5.75	6.46	42.5	275.13	7.75	7.17	642.5	463.01
Sur	4.75	5.14	17.5	29.74	4.75	5.18	17.5	30.83	5.75	6.70	42.5	205.67	5.75	7.29	17.5	346.92
Duqum	4.25	5.30	17.5	135.75	4.75	5.53	42.5	164.40	7.25	6.77	642.5	527.95	7.75	7.33	642.5	685.01
Haima	4.25	5.20	17.5	141.71	4.75	5.45	42.5	180.93	7.25	6.81	642.5	655.82	7.75	7.32	642.5	775.20
Salalah	6.75	5.88	142.5	108.90	6.25	6.07	142.5	122.10	6.75	6.44	142.5	182.90	6.75	6.48	142.5	199.50

Seismic hazards of Muscat and Sur cities are almost dominated by small to moderate earthquakes from the nearby Oman Mountains' seismic source for all spectral periods at the two selected return periods (Tables 4 and 5). Although east Makran subduction zone is the second contributing source to the total hazard at SA of 2.0 at these two cities, it does not contribute significantly to the seismic hazard. Similar behavior is observed at Rustaq City with an exception at 2.0 second at 475-year return period, where east Makran Subduction zone with larger magnitude at about 642 km controls the long period hazard.

For the two northern cities Sohar and Diba, the calculated seismic hazards are controlled by the nearby earthquakes from Oman Mountains' seismic source for short SA periods and by distant larger earthquakes from Makran and Zagros seismic zones for longer spectral periods at 475-year return period (Fig. 7). For 2475-year return period, Makran seismic zone dominates the long

Table 5 Deaggregation results in terms of mean and model magnitude and distance of the most contributing seismic source for the 12 selected cities for PGA and SA at 0.2, 1.0, and 2.0 s for 2475-year return period

City	PGA				SA (T = 0.2 s)				SA (T = 1.0 s)				SA (T = 2.0 s)			
	Magnitude		Distance		Magnitude		Distance		Magnitude		Distance		Magnitude		Distance	
	Mode	Mean	Mode	Mean	Mode	Mean	Mode	Mean	Mode	Mean	Mode	Mean	Mode	Mean	Mode	Mean
Khasab	5.25	5.78	17.5	46.58	5.75	5.79	17.5	43.25	6.75	6.47	67.5	122.40	6.75	6.95	67.5	248.10
Diba	5.25	5.42	17.5	31.09	5.25	5.46	17.5	30.14	5.75	6.44	17.5	164.74	8.25	7.14	642.5	356.99
Sohar	5.25	5.30	17.5	20.88	5.25	5.40	17.5	21.25	5.75	6.26	17.5	159.70	8.25	7.30	642.5	427.60
Buraimi	4.25	5.34	17.5	63.01	4.25	5.55	17.5	81.57	6.75	6.71	292.5	349.07	8.25	7.59	642.5	635.13
Ibri	5.75	5.45	42.5	40.59	5.75	5.52	42.5	42.74	5.75	6.64	42.5	292.30	8.25	7.68	642.5	598.77
Rustaq	5.25	5.31	17.5	20.87	5.25	5.38	17.5	21.74	5.75	6.27	17.5	133.10	5.75	7.37	17.5	414.01
Muscat	5.25	5.31	17.5	21.5	5.25	5.38	17.5	22.02	5.75	6.65	17.5	156.10	5.75	7.51	17.5	358.70
Nizwa	4.75	5.19	17.5	20.64	5.25	5.29	17.5	21.76	5.75	6.34	17.5	156.11	5.28	7.48	642.5	459.96
Sur	5.25	5.31	17.5	21.54	5.25	5.39	17.5	22.41	5.75	6.80	17.5	160.01	5.75	7.58	17.5	337.49
Duqum	4.25	5.18	17.5	44.52	4.25	5.29	17.5	50.04	8.25	6.60	642.5	303.32	8.25	7.77	642.5	752.42
Haima	4.25	5.18	17.5	44.5	4.25	5.29	17.5	49.52	8.25	6.49	642.5	321.42	8.25	7.77	642.5	818.95
Salalah	4.25	5.43	17.5	58.41	4.75	5.73	17.5	75.57	6.75	6.43	142.5	152.30	6.75	6.48	142.5	176.90

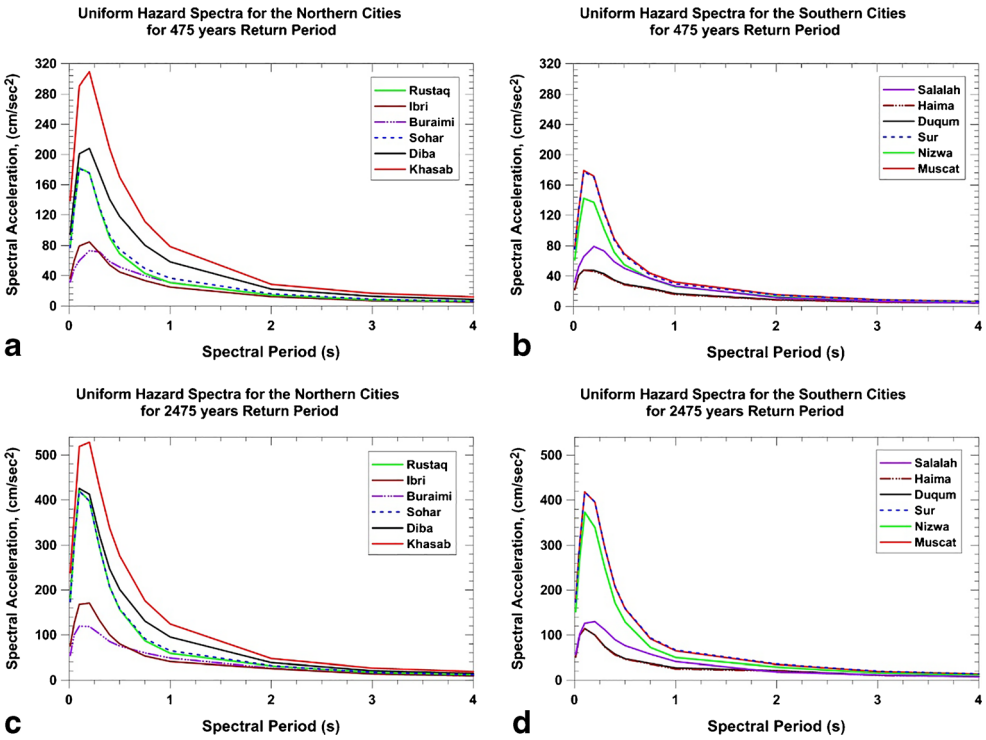

Fig. 8 Weighted average geometrical mean 5% damped horizontal component UHS at 475- and 2475-year return periods for PGA, 0.2-, 1.0-, and 2.0-s spectral periods

period hazards of the two cities. At the most northern city of Khasab, seismic hazards at all spectral periods are dominated by intermediate distance (42–97 km) earthquakes at the Arabian Gulf and Hormuz region for 475- and 2475-year return periods with minor effect from eastern Makran seismic zone. This is principally due to the low seismic activity nearby the city in comparison to Zagros seismic zones.

Table 6 Seismic hazard values at the 12 selected cities for some important spectral periods for 475- and 2475-year return periods, extracted from the UHS of each city

City	Return period	PGA	0.1 s	0.2 s	0.3 s	0.4 s	0.5 s	1.0 s	2.0 s
Khasab	475	139.0	290.8	309.2	258.5	208.1	170.1	78.6	28.7
	2475	238.3	519.1	528.6	428.1	338.1	276.2	124.4	47.6
Diba	475	94.6	201.0	208.2	174.8	140.9	118.0	58.4	22.4
	2475	183.8	425.6	412.8	321.7	247.1	201.3	95.4	38.5
Sohar	475	77.3	181.5	175.5	130.3	94.2	74.7	36.8	16.1
	2475	174.0	419.7	397.4	294.7	207.4	158.2	64.9	31.9
Buraimi	475	31.9	60.0	73.2	71.6	58.9	51.6	31.1	14.3
	2475	54.4	119.6	118.8	102.5	85.3	75.2	48.6	26.4
Ibri	475	36.5	79.4	84.8	70.1	54.3	44.9	25.0	12.3
	2475	75.3	168.1	170.9	132.3	100.3	80.1	40.8	25.5
Rustaq	475	77.5	182.3	176.0	128.5	90.7	69.1	30.8	14.4
	2475	174.1	420.2	398.0	295.1	207.4	156.4	59.2	31.1
Muscat	475	76.5	179.2	171.7	125.5	89.7	69.5	32.2	15.5
	2475	173.7	418.2	395.7	293.3	207.5	158.3	64.8	34.6
Nizwa	475	61.2	142.4	137	102.2	71.8	55.2	26	12.8
	2475	151.7	373.1	340.1	248.8	171.5	129	50	28.9
Sur	475	75.9	177.8	170.3	123.6	87.9	67.7	29.8	15.1
	2475	173.4	418.2	396	294.1	208.9	159.5	66.6	35.6
Duqum	475	22.3	48.1	47.6	43.1	34.9	29.5	16.8	8.9
	2475	50.8	114.3	100	73.9	57.3	47.2	27.2	21.2
Haima	475	21.9	47.9	46.1	41.6	34	28.6	15.8	8.4
	2475	50.8	114.4	99.9	72.5	55.5	46	24.8	20.2
Salalah	475	32.4	65.8	79.3	73.3	59.1	50.4	26.9	11.6
	2475	56.8	126.2	129.9	111.3	89.5	76.3	40.9	17.9

Uniform hazard spectra (UHS)

Uniform hazard spectrum is extensively used as a reliable illustration of earthquake actions in earthquake-resistant design codes. In this study, UHS are obtained by determining several hazard curve (one for each spectral period of interest, including PGA), utilizing above GMPEs. The value of ground-motion correspondent to each spectral period is determined for the specified return periods (herein 475 and 2475 years, respectively) and plotted versus spectral period generating UHS. In this way, the spectrum is created period by period, certifying that it provides the same hazard level along the whole range of spectral periods. Thus, UHS do not show the spectrum of a real single earthquake but rather reflect the intensity of ground motions that could be reached or exceeded for the specified return period at various spectral period.

Uniform hazard spectra on rock conditions for return periods of 475 and 2475 at the 12 selected cities are shown in Fig. 8 a and c for the six selected cities at the north of Oman and in Fig. 8 b and d for the six southern cities. Such return periods were chosen because of their importance being referenced in most recent seismic design codes. Hazard values of horizontal PGA and SA with 5% damping for 0.1, 0.2, 0.3, 0.4, 0.5, 1.0, and 2.0 s are shown in Table 6. The highest weighted average spectral accelerations are observed at spectral periods of 0.1 and 0.2 s (plateau accelerations), where the maximum difference in SA values among all sites is observed. The ratio between the plateau ground motions and PGA for 475-year return period ranges between 2.2 and 2.5, which is in consistency with the 2.5 value commonly used in earthquake-resistant designs.

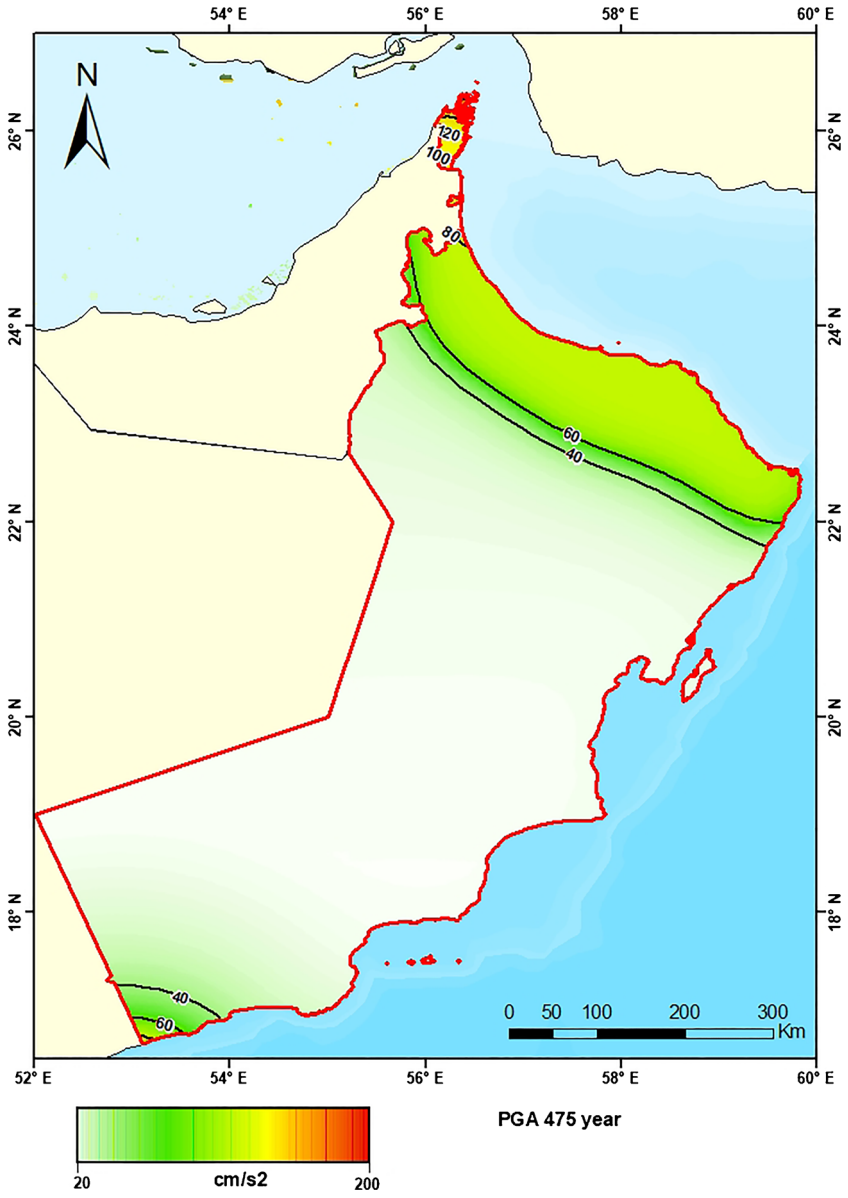

Fig. 9 Updated seismic hazard map of Oman in terms of PGA (at rock site conditions) for return period 475 years

Like the PGA hazard levels, SA values has a general tendency to increase northward with highest hazards at Khasab City, reflecting the influence of Zagros and Makran seismic zones. The maximum acceleration for 475 years of return period at Khasab City is 309 cm/s^2 at 0.2 s and about 79 cm/s^2 at 1 s, while in Muscat, the expected accelerations for 475-year return period are 172 and 32 cm/s^2 at 0.2 and 1.0 s spectral periods, respectively. The updated values denote that SA values at short periods are greater than those found in the El-Hussain et al. (2012), whereas a little bit lower SA are noticed at longer spectral periods. As the seismic source model in the two studies is almost the same, the difference in hazard values could be attributed to the more complete data set and better GMPEs used in the current study.

Seismic hazard maps

Seismic hazards were estimated at the vertices of 0.1° × 0.1° grid for return periods of 475 and 2475 years, involving the whole Sultanate of Oman. Maps were generated by calculating hazard curves at all grid points for PGA and 5% damped SA values. PGA and 5% damping SA values were thus determined at 3206 computation nodes and used to provide updated seismic hazard maps, allowing creating fairly accurate uniform hazard spectra at any vertex. Herein, only maps of geometrical mean PGA at 475- and 2475-year return periods and 5% damped SA for 0.2 s and 1 s at 475-year return period are provided (Figs. 9, 10, 11, and 12). These maps are the principal outcomes of the current study, providing the

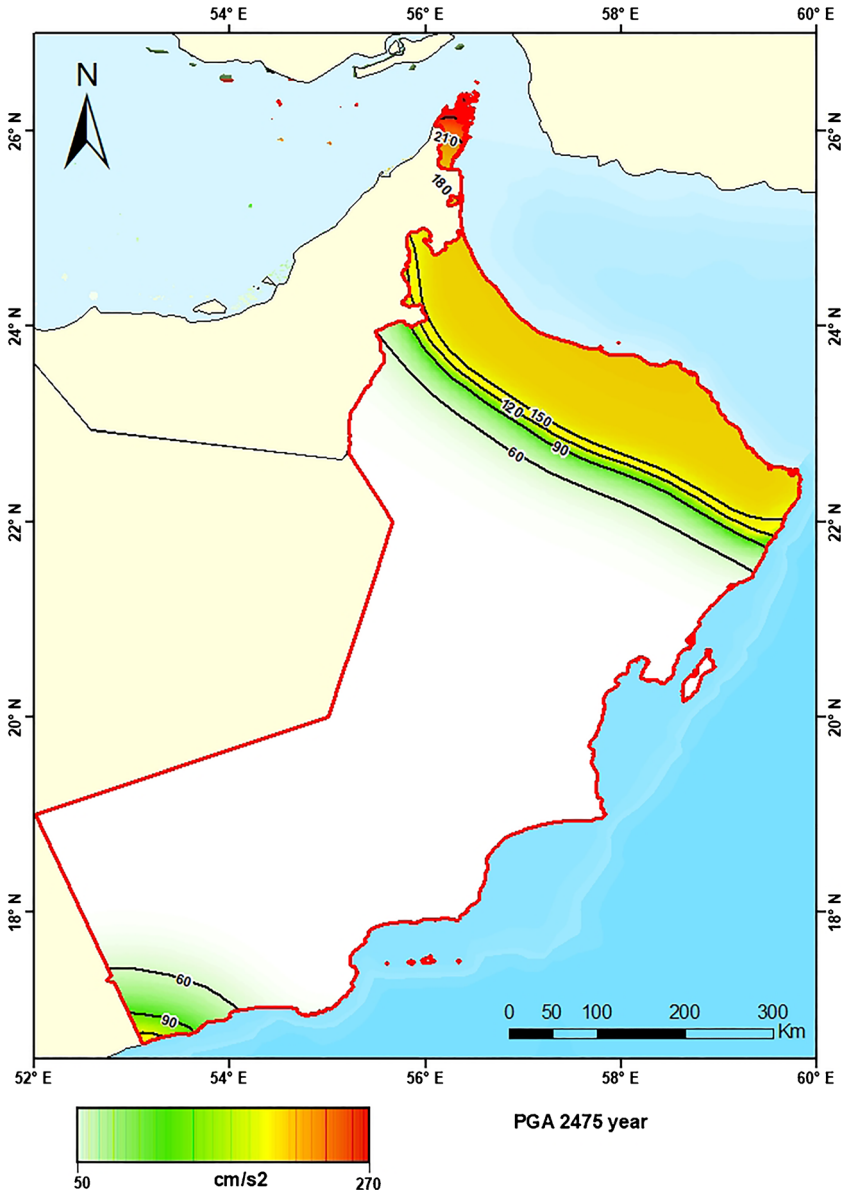

Fig. 10 Updated seismic hazard map of Oman in terms of PGA (at rock site conditions) for return period 2475 years

essential ground motions required for improving Omani seismic code, whether according to the European or American style codes.

Seismic hazard maps identify areas in the most northern parts of the country, where relatively high PGA together with SA hazards are obtained, while the remaining parts are characterized by their relatively lower hazard levels. The weighting average of PGA across the country ranges from 20 to 180 cm/s^2 for 475-year return period and from 50 to 350 cm/s^2 for 2475-year return period. Moderate PGA levels around Muscat City is attributed to the immediacy to Oman Mountains as well as Makran subduction zone. Both Oman Mountains and Arabian Peninsula are among the lowest active zones in the region, resulting in low PGA of less than 40 cm/s^2 over the majority of Omani territory (middle area). Moreover, the southern area including Salalah has hazard values up to 60 cm/s^2 for 475-year return period, which is slightly higher than the middle area due to its proximity to Alula-Fartaq seismic zone. The PGA levels for 2475-year return period are almost double those for 475-year return period at the most northern parts of the country and about 1.6 times the hazard levels at the southern areas. Comparable results are obtained in several literatures (Peláez et al. 2006; Hamdache et al. 2012; Al-shijbi et al. 2019).

In addition to the significance of 0.2 s maps in earthquake codes, it is also vital because it is the natural period of the two story buildings, which are widely spread in Oman. Maximum hazard values are observed mostly at this spectral period, which peaks in the same regions like PGA with maximum ground motions reaching 380 and 720 cm/s^2 at the most northern parts for 475- and 2475-year return periods, respectively.

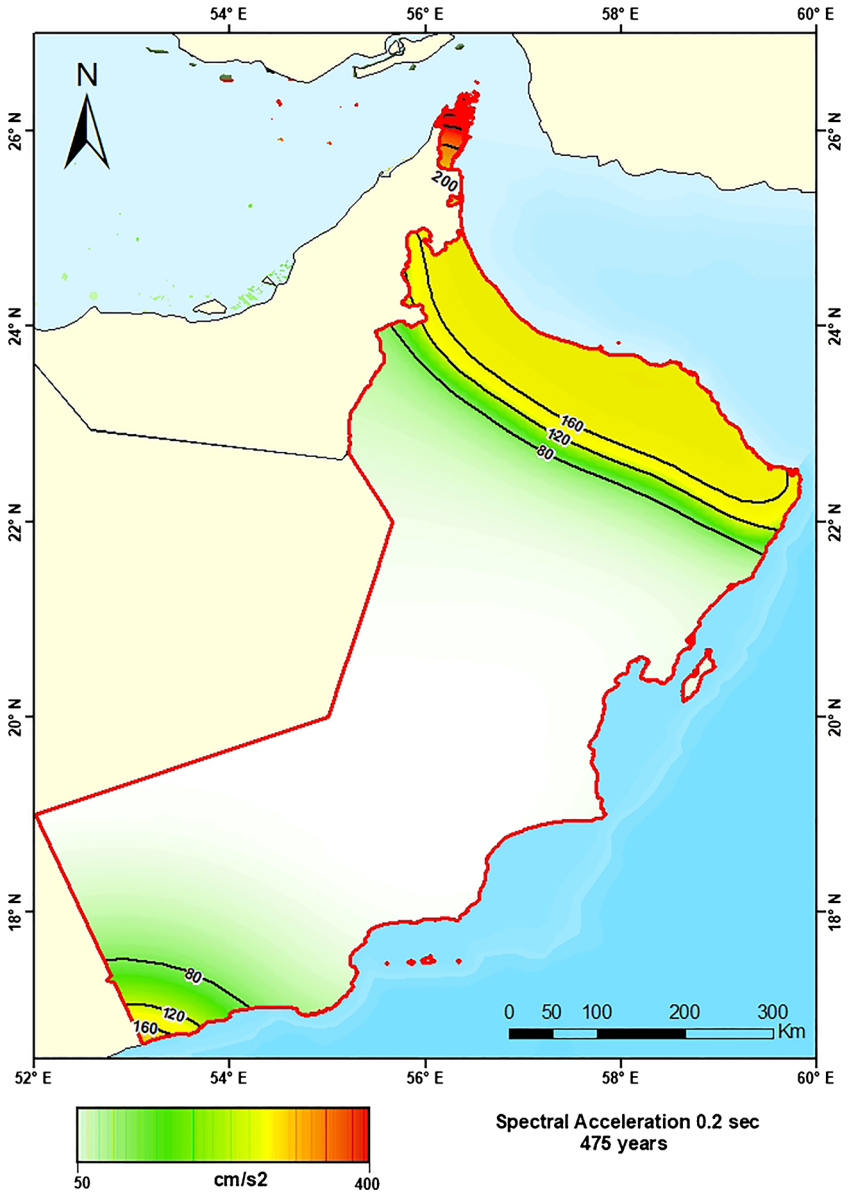

Fig. 11 Updated seismic hazard map of Oman in terms of 0.2-s spectral period (at rock site conditions) for return period 475 years

Map of 1.0-s spectral period for 475-year return period show, as expected, less hazard levels than the maps for lower spectral periods. Additionally, it is simply noticed that iso-acceleration lines in these maps are less steep gradient than those of shorter periods, confirming the faster reduction of short spectral period amplitudes with distance. Consequently, adjacent localities may have different short-period hazard values and small variations in input parameters can have a significant impact on the outcome hazard levels at the site of interest.

Discussion

The expected earthquake risk increases persistently as Oman becomes more inhabited, modernized, and industrialized, leading to an increase in the total exposure and thus more loses. Therefore, hazard identification and evaluation are important steps to reduce the consequent risks. Our seismic hazard results clearly show that most of Oman does not need specific seismic designs as it is characterized with low hazard levels, in consistence with the previous results. Seismic hazard maps, as well as UHS, show that the north part of the country has relatively higher hazard levels than the southern and middle parts, indicating the larger contribution of Zagros seismic zones than the local seismic sources on the total hazard. Current seismic hazard maps enable engineers to build their fairly accurate UHS at any vertex of the used grid at the bedrock conditions, leading to more enhanced earthquake-resistant designs and more secure installations.

The tendency of the hazard curves to coincide at long return periods for cities away from the most north part of Oman indicates that the low active seismic sources of Oman

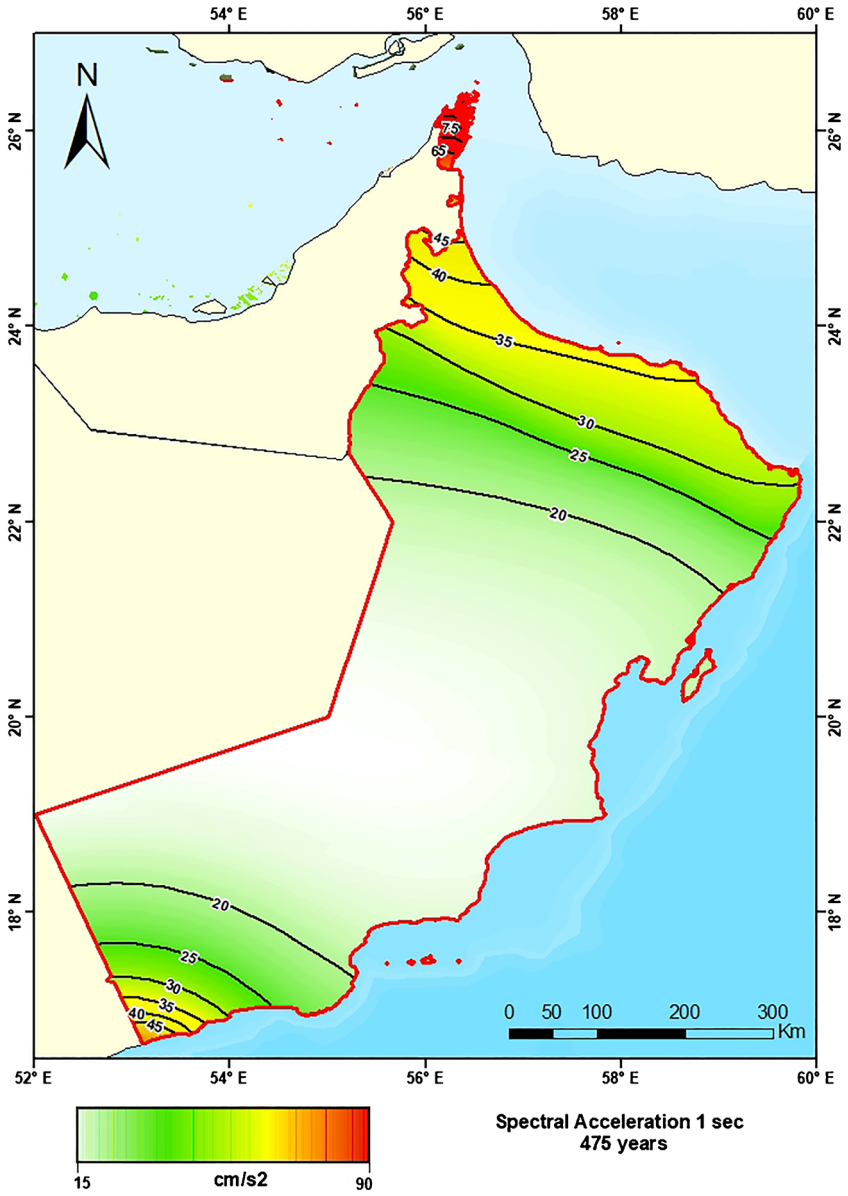

Fig. 12 Updated seismic hazard map of Oman in terms of 1.0-s spectral period (at rock site conditions) for return period 475 years

Mountains and Arabian background dominate the hazard at most investigated cities.

Uniform hazard spectra at the 12 investigated cities show some differences in shape for all spectral periods, implying that different seismic sources dominate various spectral periods.

Seismic hazard values provided in the present study are the minimum that should be utilized for earthquake resistant designs and may be considered as the ground acceleration at the bedrock level. The final design ground motion could be amplified due to the site conditions (geology and topography) and based upon the dynamic characteristics of the structure. The present study did not consider the site effect on the ground motion as it calculates the seismic hazard at the bedrock conditions. Therefore, structures located on site different from the rock conditions may suffer greater damage due to earthquake shaking. The best practice is to combine the values on maps with the site-specific characteristics in order to fully obtain the precise seismic design coefficients. Additionally, areas with high groundwater level, particularly along the coasts, may have the potential to liquefy during the earthquake actions (e.g., El-Hussain et al. 2018).

Relatively large earthquakes at Sohar, Qalhat, Nizwa, Al-Kamil, and Masafi warn for the future urbanization of Oman. These events point to the possibility of serious seismic hazard existence. Therefore, paleoseismic investigations at the regions of these reported events are important to confirm or deny the historical reports, particularly when great uncertainties are associated with many of them. Then, hazard results may be changed considerably for specific regions when causative faults are delineated and the recurrence parameters are calculated specifically for them.

Conclusions

This study provides updated national seismic hazard maps in terms of horizontal PGA and 5% damped for return periods of 475 and 2475 years at bedrock conditions in Oman. Additional efforts over previous work have been carried out to an enhanced seismic hazard model based upon, an updated earthquake database, an updated seismic source model, better ground motion prediction equations, and improved treatment of uncertainties. The majority of the Sultanate depicts low to moderate seismic hazard values. The highest hazard is observed in the northern part of Oman and decreases towards the middle parts with PGA values less than 40 cm/sec^2 for 475 years return period. Regardless of the low earthquake activity of the country, seismic hazard results have been deaggregated to depict the contribution of different magnitude-distance scenarios to the total seismic hazard. Generally, distant seismic sources with larger seismic events contribute for most sites at long spectral periods, while nearby seismic sources dominate the hazard for short spectral periods for the two selected return periods. Furthermore, seismic hazard is presented in terms of hazard curves and unified hazard spectra for 12 selected cities. Current hazard results were compared with those of the previous study of El-Hussain et al. (2012). The two studies show relatively high hazard levels to the north of the country although the updated hazards denote higher short periods SA levels.

Acknowledgments We would like to all the staff of the Earthquake Monitoring Center at Sultan Qabbos University for their kind collaboration and assistance, especially Amna Al-Dairi and Aziza Al-Manthari for handling the illustrations and tables of this study.

References

Akkar S, Bommer JJ (2010) Empirical equations for the prediction of PGA, PGV and spectral accelerations in Europe, the Mediterranean region and the Middle East. Seismol Res Lett 81: 195–206

Aldama B, Bommer JJ, Fenton CH, Staford PJ (2009) Probabilistic seismic hazard analysis for rock sites in the cities of Abu Dhbi, Dubai and Ra's Al Khymah, United Arab Emirates. Georisk 3:1–29

Al-shijbi Y, El-Hussain I, Deif A, Al-Kalbani A, Mohamed AME (2019) Probabilistic Seismic Hazard Assessment for the Arabian Peninsula. Pure Appl Geophys 176:1503–1530

Ambraseys NN, Melville CP (1982) A history of Persian earthquakes. Cambridge University Press, Cambridge

Ambraseys NN, Melville CP, Adams RD (1994) The seismicity of Egypt, Arabia and Red Sea. Cambridge University Press, Cambridge

ArRajehi A, McClusky S, Reilinger R, Daoud M, Alchalbi A, Ergintav S, Gomez F, Sholan J, Bou-Rabee F, Ogubazghi G, Haileab B, Fisseha S, Asfaw L, Mahmoud S, Rayan A, Bendik R, Kogan L (2010) Geodetic constraints on present-day motion of the Arabian Plate: Implications for Red Sea and Gulf of Aden rifting. Tectonics 29: TC3011

Atkinson GM, Boore DM (2003) Empirical ground-motion relations for subduction-zone earthquakes and their application to Cascadia and other regions. Bull Seismol Soc Am 93:1703–1729

Atkinson GM, Boore DM (2006) Earthquake ground-motion prediction equations for Eastern North America. Bull Seismol Soc Am 96: 2181–2205

Baker C, Jackson J, Priestley K (1993) Earthquakes on the Kazerun line in the Zagros Mountains of Iran: strike-slip faulting within a fold-and-thrust belt. Geophys J Int 115:41–61

Berberian M (1995) Master 'blind' thrust faults hidden under the Zagros folds, active basement tectonics and surface morphotectonics. Tectonophysics 241:193–224

Beyer, K., and Bommer, J.J., (2006) Relationships between median values and between aleatory variabilities for different definitions of the horizontal component of motion. Bulletin of Seismological Society of America 96, 1512-1522, Erratum (2007) 97, 1769.

Bommer JJ, Scherbaum F, Bungum H, Cotton F, Sabetta F, Abrahamson NA (2005) On the use of logic trees for ground-motion prediction equations in seismic hazard analysis. Bull Seismol Soc Am 95:377–389

Bosworth W, Huchon P, McClay K (2005) The Red Sea and the Gulf of Aden Basins. J Afr Earth Sci 43:334–378

Burkhard M, Grunthal G (2009) Seismic source zone characterization for the seismic hazard assessment project PEGASOS by the Expert Group 2 (EG 1b). Swiss J Geosci 102:149–188

Campbell K (2003) Prediction of strong ground-motion using the hybrid empirical method and its use in the development of ground-motion (attenuation) relations in Eastern North America. Bull Seismol Soc Am 93:1012–1033

Chiou BS, Youngs RR (2008) An NGA model for the average horizontal component of peak ground motion and response spectra. Earthquake Spectra 24:173–215

Coleman RG (1993) Geologic evolution of the Red Sea. Oxford Monographs on Geology and Geophysics 24. Oxford University Press, Oxford

Coppersmith KJ, Youngs RR (1986) Capturing uncertainty in probabilistic seismic hazard assessments within intraplate tectonic environments. In: Proceedings of the Third US national conference on earthquake engineering, vol 1, pp 301–312

Cornell CA (1968) Engineering seismic risk analysis. Bull Seismol Soc Am 18:1583–1606

Cornell CA (1971) Probabilistic analysis of damage to structures under seismic loads. In: Howells DA, Haigh IP, Taylor C (eds) Dynamic waves in civil engineering. Proceedings of a conference organized by the Society for Earthquake and Civil Engineering Dynamics. New York, John Wiley, pp 473–493

Cornell CA, Vanmarcke EH (1969) The Major Influences on Seismic Risk. In: Proceedings of the Fourth World Conference of Earthquake Engineering, 1. Santiago, Chile, pp 69–83

Deif A, El-Hussain I (2012) Seismic moment rate and earthquake mean recurrence interval in the major tectonic boundaries around Oman. J Geophys Eng 9:773–783

Deif A, El-Hussain I, Al-Jabri K, Toksoz N, El-Hady S, Al-Hashmi S, Al-Toubi K, Al-Shijbi Y, Al-Saifi M (2013) Deterministic seismic hazard assessment for Sultanate of Oman. Arab J Geosci 6:4947–4960

Deif A, Al-Shijbi Y, El-Hussain I, Ezzelarab M, Mohamed AME (2017) Compiling an earthquake catalogue for the Arabian Plate, Western Asia. J Asian Earth Sci 147:345–375

Delavaud E, Cotton F, Akkar S, Scherbaum F, Danciu L, Beauval C, Drouet S, Douglas J, Basili R, Sandikkaya MA, Segou M, Faccioli E, Theodoulidis N (2012) Towards a ground-motion logic tree for probabilistic seismic hazard assessment in Europe. J Seismol 16: 451–473

DeMets C (2008) Arabia's slow dance with India. Nature Geoscience 1: 10–11, der Schweiz, PhD thesis, ETH-Zurich.

Douglas J, Akkar S, Ameri G, Bard PY, Bindi D, Bommer J, Bora SS, Cotton F, Derras B, Hermkes M, Kuehn NM, Luzi L, Massa M, Pacor F, Riggelsen C, Sandıkkaya MA, Scherbaum F, Stafford PJ, Traversa P (2014) Comparisons among the five ground-motion models developed using RESORCE for the prediction of response spectral accelerations due to earthquakes in Europe and the Middle East. Bull Earthq Eng, Springer Verlag 12:341–358

El-Hussain I, Deif A, Al-Jabri K, Toksoz N, El-Hady S, Al-Hashmi S, Al-Toubi K, Al-Shijbi Y, Al-saifi M, Kuleli S (2012) Probabilistic seismic hazard maps for Sultanate of Oman. Nat Hazards 64:173–210

El-Hussain I, Deif A, Al-Jabri K, Mohamed AME, Al-Rawas G, Toksöz MN, Sundararajan N, El-Hady S, Al-Hashmi S, Al-Toubi K, Al-Saifi M, Al-Habsi Z (2013) Seismic microzonation for Muscat region, Sultanate of Oman. Nat Hazards 69:1919–1950

El-Hussain I, Al-Shijbi Y, Deif A, Mohamed AME, Ezzelarab M (2018) Developing a seismic source model for the Arabian Plate. Arab J Geosci 11:435

Giardini D, Grunthal G, Shedlock KM, Zhang PZ (1999) The GSHAP global seismic hazard map. Ann Geofis 42:1225–1230

Gutenberg B, Richter CF (1956) Magnitude and Energy of Earthquakes. Ann Geofis 9:1–15

Hamdache M, Peláez JA, Talbi A, Mobarki M, López Casado C (2012) Ground-motion hazard values for Northern Algeria. Pure Appl Geophys 169:711–723

Hessami K, Koyi H, Talbot C (2001) The Significance of the Strike-Slip Faulting in the Basement of the Zagros Fold and Thrust Belt. J Pet Geol 24:5–28

Hessami K, Nilforoushan F, Talbot CJ (2006) Active deformation within the Zagros Mountains deduced from GPS measurements. J Geol Soc 163:143–148

Kijko A (2004) Estimation of the maximum earthquake magnitude Mmax. Pure Appl Geophys 161:1655–1681

Kijko A, Sellevoll MA (1992) Estimation of earthquake hazard parameters from incomplete data files Part II: Incorporation of magnitude heterogeneity. Bull Seismol Soc Am 82:120–134

Kopp C, Fruehn J, Flueh ER, Reichert C, Kukowski N, Bialas J, Klaeschen D (2000) Structure of the Makran subduction zone from wide angle and reflection seismic data. Tectonophys 329:171–191

Kramer SL (1996) Geotechnical Earthquake Engineering. Prentice Hall, Upper Saddle River

Kusky T, Robinson C, El-Baz F (2005) Tertiary-Quaternary faulting and uplift in the northern Oman Hajar Mountains. J Geol Soc 162:871–888

McGuire RK (1978) FRISK: Computer program for seismic risk analysis using faults as earthquake sources. U.S. Geological Survey Open-File Report 78-1007.

Mohamed ME, Deif A, El-Hadidy S, Moustafa Sayed SR, El Werr A (2008) Definition of soil characteristics and ground response at the northwestern part of the Gulf of Suez, Egypt. J Geophys Eng 5:420–437

Musson RMW (2009) Subduction in the Western Makran: the historian's contribution. J Geol Soc Lond 166:387–391

Peláez JA, Hamdache M, López Casado C (2006) Seismic hazard in terms of spectral accelerations and uniform hazard spectra in Northern Algeria. Pure Appl Geophys 163:119–135

Reilinger R, McClusky S, Vernant P, Lawrence S, Ergentav S, Cakmak R, Ozener H, Kadirov F, Guliev I, Stepanyan R, Nadariya M, Hahubia G, Mahmoud S, Sakr K, ArRajehi A, Paradissis D, Al-Aydrus A, Prilepin M, Guseva T, Evren E, Dmitrotsa A, Filikov SV, Gomez F, Al-Ghazzi R, Karam G (2006) GPS constraints on continental deformation in the Africa-Arabia-Eurasia continental collision zone and implications for the dynamics of plate interactions. J Geophys Res 111:B05411

Toro GT (2006) The effects of ground-motion uncertainty on seismic hazard results: Examples and approximate results. Annual Meeting of the Seismological Society of America, San Francisco

Uhrhammer R (1986) Characteristics of northern and southern California seismicity. Earthquake Notes:57–61

Vernant PH, Nilforoushan F, Hatzfeld D, Abassi MR, Vigny C, Masson F, Nankali H, Martinod J, Ashtiani A, Bayer R, Tavakoli F, Chery J (2004) Present-day crustal deformation and plate kinematics in Middle East constrained by GPS measurements in Iran and northern Oman. Geophys J Int 157:381–398

Youngs RR, Chiou SJ, Silva WJ, Humphrey JR (1997) Strong ground motion attenuation relationships for subduction zone earthquakes. Seismol Res Lett 68:58–73

Zhao JX, Zhang J, Asano A, Ohno Y, Oouchi T, Takahashi T, Ogawa H, Irikura K, Thio HK, Somerville PG, Fukushima Y (2006) Attenuation relations of strong ground motion in Japan using site classification based on predominant period. Bull Seismol Soc Am 96:898–913